

Special Section:

Coastal hydrology and oceanography

Key Points:

- Relaxation periods between upwelling events generate poleward transport of warm and oxygen-rich shelf waters
- Internal waves generate daily to infra-daily oscillations of oxygen over a density-stratified shelf during the warm season
- Mid-shelf dissolved oxygen reflects open ocean properties with changes consistent with estimated respiration rates during upwelling season

Supporting Information:

Supporting Information may be found in the online version of this article.







Correspondence to:A. W. Tall,
abdoulwahab.tall@ucad.edu.sn**Citation:**

Tall, A. W., Machu, E., Echevin, V., Capet, X., Pietri, A., Corréa, K., et al. (2021). Variability of dissolved oxygen in the bottom layer of the southern Senegalese shelf. *Journal of Geophysical Research: Oceans*, 126, e2020JC016854. <https://doi.org/10.1029/2020JC016854>

Received 22 APR 2020

Accepted 9 MAY 2021

Variability of Dissolved Oxygen in the Bottom Layer of the Southern Senegalese Shelf

 A. W. Tall¹ , E. Machu^{1,2} , V. Echevin³ , X. Capet³ , A. Pietri^{3,4} , K. Corréa^{1,2}, S. M. Sall¹, and A. Lazar³ 

¹Laboratoire de Physique de l'Atmosphère et de l'Océan Siméon Fongang, Université Cheikh Anta DIOP de Dakar, Ecole Supérieure Polytechnique, Dakar, Sénégal, ²Université de Bretagne Occidentale, CNRS, IRD, Ifremer, Laboratoire d'Océanographie Physique et Spatiale (LOPS), IUEM, Brest, France, ³LOCEAN-IPSL, IRD/CNRS/Sorbonne Université (UPMC)/MNHN, UMR 7159, Paris, France, ⁴Instituto del Mar del Peru (IMARPE), Esquina General Gamarra y Valle, Callao, Perú

Abstract The observation station “Melax” was deployed in 2015 on the wide and shallow south Senegalese shelf to study the ocean dynamics, air-sea interactions, and dissolved oxygen (DO) cycle. Data from February 2015 to August 2016 were used to study the main physical processes affecting the variability of DO in the bottom layer (~30 m depth) on time scales ranging from tidal to seasonal. Between November and May, wind-driven upwelling provides phytoplankton enrichment of the surface layers and brings cold, salty, and depleted DO on the shelf. Water properties at Melax vary depending on the source waters located at the shelf edge. The DO concentration changes between the shelf edge and Melax are broadly consistent with the inferred respiration rates estimated in previous studies. In contrast, the monsoon season (July–October) is characterized by weak westerly winds and northward currents. Bottom waters are warmer, fresher, and more oxygenated. The slower circulation in this period allows a stronger decoupling between the water properties of the waters observed at Melax and those of the source waters. Stratification strengthening near the bottom layer inhibits vertical mixing and induces strong high-frequency variability in properties caused by internal tide-generated waves. Intense upwelling events can deepen the mixed layer and intermittently transform the bottom layer waters (locally or remotely). Relaxation events associated with current reversals significantly modify their properties. Coastal trapped waves constitute a distant forcing that can act year-round, impacting both shelf waters and source regions.

Plain Language Summary Global warming and extra nutrient loads from agriculture and waste-waters reduce the oxygen content in the ocean. Incidentally, oxygen-depleted waters are encountered with increased frequency oceanwide and this trend is more pronounced in coastal environments. Temperature and oxygen impact the metabolism of marine organisms and their variations can be major sources of (natural or anthropogenic) stresses. We used here measurements made at a fixed monitoring buoy (Melax) located over the southern Senegalese mid-shelf (35 m depth) to study the variability of bottom oxygen (the surface being well oxygenated). Its seasonality is constrained by the circulation and the wind regime. They induce the transport of deep, colder, saltier, and less oxygenated waters from the shelf break onto the shelf during the upwelling season compared to the monsoon season. The properties of water masses on the shelf thus depend on those of the water masses drawn from the open ocean through the shelf break which can be modified by many processes acting over a wide range of scales from days to seasons and longer. On the shelf, respiration of organic matter reduces oxygen whereas diurnal wind variability and internal tides oxygenate bottom layers when the water column is stratified.

1. Introduction

Hypoxia/anoxia events are becoming more and more frequent in coastal areas (Gilbert et al., 2010) in a context of deoxygenation of the global ocean (Breitburg et al., 2018). When seawater dissolved oxygen (DO) reaches hypoxic levels (~50–65 $\mu\text{mol kg}^{-1}$), this can have significant consequences on coastal ecosystems, such as fish mortality events (e.g., Vaquer-Sunyer & Duarte, 2008), decrease in the biodiversity of benthic fauna (Conley et al., 2007), and habitat modification (Levin & Breitburg, 2015). Like many coastal regions, the West African (WA) seaboard, located on the eastern margin of the Atlantic oxygen minimum zone (OMZ) (Brandt et al., 2015; Voituriez & Chuchla, 1978), is also prone to deoxygenation: hypoxic oxygen

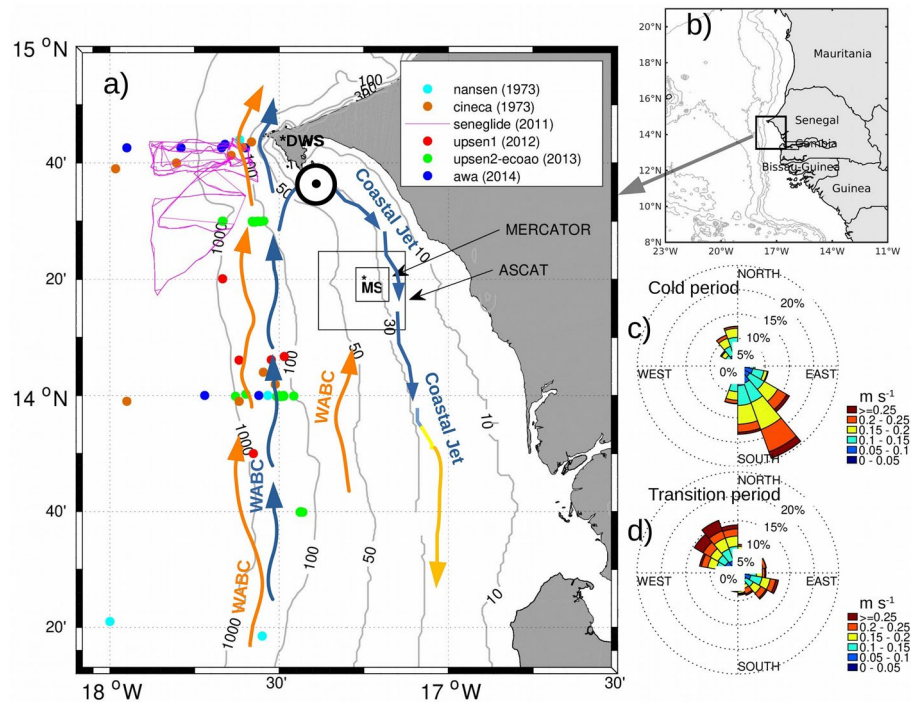


Figure 1. Presentation of the study area: (a) bottom topography and coastline in the south Senegalese sector: the 10, 30, 50, 100, and 1,000 m isobaths are represented by gray lines. The Melax station (MS, 14°20.8'N-17°13.68'W) is represented by a black star. The two black squares around MS represent the ASCAT wind stress (1/4°) and MERCATOR PSY4V2 model (1/12°) grid points respectively. The Yoff weather station at Dakar airport (located at 27 m above ground) is represented by a black star (DWS). The colored circles off the shelf mark the location of the T/S/DO profiles from the NANSEN (1973, cyan), CINECA (1973, brown), UPSEN1 (2012, red), UPSEN2-ECOAO (2013, green), and AWA (2014, blue) campaigns. The trajectory of the glider cruise collecting T/S/DO in 2011 is represented in magenta. The poleward Western African boundary Current (WABC) is represented by arrows oriented northward during the upwelling cold period (blue arrow) and the transition period (orange arrows). Blue arrows oriented southwards indicate equatorward advection of coastal waters from the upwelling center (see symbol south of Dakar around 14°35'; Ndoye et al., 2017) during upwelling events. The gradual warming of shelf waters advected southwards is indicated by the blue-yellow-orange arrow; (b) location of the south-Senegalese shelf in West Africa; Compass card of ADCP currents at Melax (28 m depth) during (c) the 2015 and 2016 cold periods (February 12–April 23) and (d) the transition period (November 25, 2015–February 10, 2016). The current frequency (resp. velocity) in these compasses is represented by a percentage (resp. color). The isobath direction at the Melax buoy position is oriented northwest/southeast (−30°).

levels (50–65 $\mu\text{mol kg}^{-1}$) have recently been measured over the Mauritanian (Brandt et al., 2015; Klenz et al., 2018; Thomsen et al., 2019) and Senegalese (Capet et al., 2017) shelves, offshore of WA. An episode of extreme deoxygenation (anoxia) has even been observed off Senegal (Machu et al., 2019). However, DO levels are generally higher there than in eastern Pacific coastal systems because the Atlantic OMZ is more oxygenated than the Eastern Pacific one (e.g., Brandt et al., 2015). Outside these circumstantial evidence, little is known about the distribution of DO over the WA shelves and its temporal variability. For instance, the frequency of hypoxic/anoxic events, their typical duration and seasonality, the processes implicated in low DO occurrences are presently unknown. This makes it difficult to anticipate the potential long-term trends in DO levels and variability, for example, in relation to climate change.

Along the Senegalese shelf, the upwelling of cold, nutrient-rich sub-surface waters occurs from November to May under the influence of intermittent upwelling favorable northerly winds (Ndoye et al., 2014; Roy et al., 1989). Coastal upwelling is intensified south of the Cape Verde peninsula, generating a south-south-eastward flow over the shelf (Ndoye et al., 2017; Figure 1). The rise of nutrient-replete deep waters in the euphotic layer promotes the growth of phytoplankton near the coast (Lathuilière et al., 2008). Upwelling source waters originate from the shallow (~100 m depth) part of the OMZ located along the continental slope of Mauritania and Senegal (Ndoye et al., 2017). Whereas the surface layer is generally near or above saturation levels as a result of photosynthesis and exchanges with the atmosphere, the bottom layer

of the outer shelf is thus supplied with DO-depleted waters ($\sim 50\text{--}60\ \mu\text{mol kg}^{-1}$), as typically found in Eastern Boundary Upwelling Systems (hereafter EBUS; e.g., Chapman & Shannon, 1985; Pitcher & Probyn, 2010, 2011 in the Benguela; Checkley & Barth, 2009 in the California upwelling system). However, the rate of supply and the DO concentrations of upwelling source waters may vary with the environmental conditions. Notably, the WA upwelling system is influenced by seasonal and intraseasonal coastal trapped waves (CTWs) propagating toward the north (Diakhaté et al., 2016; Kounta et al., 2018; Polo et al., 2008). The influence of CTWs on the oxycline depth over the continental slope and shelf has been highlighted in other EBUS (e.g., Espinoza-Morriberón et al., 2019, off Peru; and Monteiro et al., 2011, off Benguela). In addition to displacing the oxycline vertically, horizontal currents associated with CTWs carry water masses alongshore: an equatorward current associated with a downwelling CTW may bring warmer, fresher and more oxygenated water onto the shelf (Brandt et al., 2015; Schütte et al., 2016).

The transition periods (May–July) from the upwelling season to the warm and rainy monsoon season (July–September) have been less studied. During this time period, equatorward wind decreases gradually, shelf waters get warmer and more stratified, and incursions of the poleward WA Boundary Current over the shelf become frequent (Kounta et al., 2018; Figure 1). During the monsoon season, upwelling is strongly reduced or halted (Ndoye et al., 2014) which tends to reduce wind-driven mixing rates. The shelf and upper continental slope currents reverse to poleward, which brings freshwater of riverine origin (Rebert, 1982) and oxygen-rich near-surface waters from the south (Voituriez & Chuchla, 1978) onto the shelf and enhances water column stratification in our study region. The primary production regime changes with lower enrichment rates and dominance of subsurface phytoplankton maxima (Voituriez & Dandonneau, 1974). Hence, conditions during the monsoon season can impact near-bottom DO values in either direction.

At shorter daily to intradaily time scales, other processes may affect DO concentrations on the shelf. For instance, mixing during peak winds can ventilate bottom layers depleted in DO (Capet et al., 2017) through bursts of intense vertical mixing involving oxygenated near-surface waters (Touré, 1983). Tidal currents may contribute to the high-frequency (HF) variability of DO by horizontal advection of DO gradients (e.g., Adams et al., 2013 for the Oregon shelf). Furthermore, the interaction between bathymetry and barotropic tide generates internal tidal waves that propagate over the southern part of the Senegalese shelf (Capet et al., 2017). DO can then be modulated by the vertical (reversible) displacement of the oxygen gradient associated with the passage of internal waves (Adams et al., 2013). Internal waves can also induce offshore water intrusions under the thermocline on the continental shelf (Nam & Send, 2011; Wong et al., 2012) and mixing by breaking (Capet et al., 2017; Moum et al., 2003).

In the spirit of Adams et al. (2013), and as an incremental step beyond Capet et al. (2017) and Machu et al. (2019), a DO time series collected from February 2015 to August 2016 at the location of a fixed mid-shelf air-sea monitoring buoy named “Melax” (lightning in Wolof) is studied. The mooring is located at $14^{\circ}20.8'N\text{--}17^{\circ}13.68'W$ over the Senegalese shelf (35 m depth, Figure 1). The oxygen sensor is located ~ 7 m above the sea floor. Physical ancillary data (currents, temperature, and salinity in most of the water column) are also available. Near-bottom DO variability is documented over the widest possible range of temporal scales, from super-inertial to seasonal. Despite some data gaps, the ancillary data allow us to make plausible inferences on the processes responsible for the DO variability at different scales. Note that we do not have direct measurements of respiration rates. Indirect ballpark estimates will be provided based on different assumptions but focus will mainly be on physical processes. Overall, the main scale-dependent questions we address in this study are the following: which are the major physical processes driving the observed DO fluctuations at seasonal to intraseasonal/synoptic scale? To which extent do biogeochemical processes contribute to the observed DO variability?

The paper is structured as follows: we present the mooring data, historical data from short-term cruises, and the methods used to process and filter the data in Section 2. In Section 3, we analyze the seasonal and intraseasonal variability of oxygen and various variables characterizing the environment (wind, currents, temperature, salinity, chlorophyll-*a* [Chl-*a*] from satellite). The origin of water masses, the variability of oxygen at different time scales, and the relationships between the different environmental variables are carefully examined. Section 4 presents a discussion of the main findings. Section 5 concludes and gives some research perspectives.

Table 1
Description of the Observations Recorded at Melax Station

| Variable | Depth (m) | Sensor | Interval (min) | Time periods |
|--------------------------|---|---|----------------|---|
| Dissolved oxygen | 28 | PME miniDO ₂ T | 10 | Feb 11–Apr 23, 2015 Oct 14, 2015–Aug 01, 2016 |
| Temperature | 28 | PME miniDO ₂ T | 10 | Feb 11–Apr 23, 2015 Oct 14, 2015–Aug 01, 2016 |
| Temperature | 4; 6 1; 8; 10; 12; 14 18; 21; 24; 28 | SBE56 thermistors RBR TR thermistors | 0.5 | Feb 11, 2015–Apr 26, 2016 |
| Temperature | 35 | SBE37 CTD | 90 | Nov 26, 2015–Apr 26, 2016 |
| Temperature and salinity | 28 | SBE37SM CTD | 2 5 | Feb 11, 2015–Apr 26, 2016 Apr 26–Aug 01, 2016 |
| Current | 28 | AquaPro 600 khz | 90 60 | Feb 11–Jun 16, 2016 Nov 26, 2015–Apr 26, 2016 Apr 26–Jun 10, 2016 |
| Wind speed and direction | 2 m above sea level | 05106 Wind Monitor—MA | 10 | Feb 11–Aug 30, 2015 Oct 16, 2015–Apr 26, 2016 Apr 26–Aug 01, 2016 |

Notes. The measured variables, the depths of measurement, the model of sensor, the sampling frequency, and the measurement periods are presented. Wind speed and direction are measured at 2 m height on the buoy. The ADCP measured the current between 2 and 33 m depth (1-m-thick cells) but only the measurements at 28 m are showed.

2. Data and Methods

2.1. Melax Station

The Melax observatory buoy was deployed on February 11, 2015 at 14°20.8′N-17°13.68′W by A. Lazar and D. Dausse by 35 m depth near the main upwelling cell of the southern Senegalese shelf (Ndoye et al., 2017) (Figure 1). Among the atmospheric and oceanographic sensors mounted on the buoy (<https://sites.google.com/site/jointinternationallabeclairs/melax>), surface wind (2 m above sea surface), temperature, salinity, DO, and current measurements were used in this study (Table 1). Sea-Bird SBE37 conductivity-temperature-depth (CTD) recorded conductivity, temperature, and pressure at 28 m depth from February 11, 2015 to the end of April 2016 and then from May 2016 to August 2016, at respectively 2 and 5 min intervals (see Table 1). DO was measured at 10 min interval at 28 m by miniDO₂T sensors (DO and temperature) deployed successively on February 11, 2015, October 14, 2015, and April 26, 2016. The logger collected measurements of DO with an accuracy of ±5% and temperature to ±0.1 °C. The number of measurements performed by each sensor was much less than the half-million measurements beyond which a re-calibration is recommended by the manufacturer. An RBR thermistor chain measured temperatures every 30 s at 11 different depths. Three periods of current measurement were carried out using an ADCP (acoustic Doppler current profiler) AquaPro 600 kHz which was calibrated before and after each deployment. ADCP measurements are used at 28 m, the depth of the oxygen sensor. The ADCP calibration coefficients were calibrated by standard calibration procedures (Pollard & Read, 1989). We also used the ADCP temperature sensor (accuracy of 0.1 °C and a resolution of 0.01 °C) to represent bottom temperature.

2.2. Ancillary Data

2.2.1. Glider Observations

An autonomous underwater vehicle, the deep glider Hannon (<https://www.ego-network.org/dokuwiki/doku.php?id=public:plotdeployment&glid=2&dId=207>), was deployed west of Dakar by A. Lazar, P. Estrade, and the Everyone's Gliding Observatories team from February 8 to March 17, 2011. During these 5 and a half weeks, the glider sampled 725 vertical profiles from the surface to 800 m depth along a 650 km

long track in the latitude range 14.2°–15.1°N and the longitude range 17.4°–17.9°W. The horizontal resolution along its track is ~0.9 km and the data were recorded at a temporal resolution of 0.5 Hz which corresponds to about 0.5 dbar at the diving speed of the glider. The data are then interpolated on a 1 dbar vertical grid. The glider was equipped with an unpumped Sea-Bird CTD cell that generally needs to be corrected for the thermal mass of the conductivity cell in order to obtain a precise salinity. The neighboring ascending and descending profiles collected at the beginning of the mission were used to identify the time lag that minimizes the differences in salinity between them (Garau et al., 2011; Pietri et al., 2013).

An Aanderaa optode was mounted on the tail of the glider to measure DO concentrations. The oxygen sensor calibration was performed using 36 oxygen profiles (18 pairs of up and down casts) recorded at the beginning of the deployment. To correct for the time delay of the optode, DO data are recomputed using the CTD temperature data with a time lag that minimizes the difference of oxygen in up and down casts (Kolodziejczyk et al., 2018; Thomsen et al., 2016). The average difference between up and down pairs of calibrated oxygen profiles is $\sim 4.0 \pm 7.2 \mu\text{mol kg}^{-1}$ while the average difference between consecutive down casts is $\sim 4.5 \pm 9.2 \mu\text{mol kg}^{-1}$. The weak difference between those values gives confidence that the calibration correctly removed any systematic problem that could be due to the glider's displacement itself. During the rest of the deployment, data were only recorded during the descent of the glider.

Unfortunately no parallel measurements sufficiently close in time and space exist for cross calibration of oxygen data. However the Aanderaa optode 5013 mounted on the glider was a multipoint factory calibrated in March 2010, less than a year prior to its deployment (Tengberg & Hovdenes, 2014).

2.2.2. Field Surveys

Temperature, salinity, and oxygen data collected during several research cruises are also used in this study (Figure 1), in particular to report on existing conditions at the edge of the shelf along the continental slope. These cruises were carried out at periods prior to the date of deployment of the buoy during the upwelling seasons of 2012 (February 7–17, UPSEN1, chief scientist A. Lazar), 2013 (February 21–March 18, UPSEN2-ECOAO, chief scientist X. Capet), and 2014 (February 28–March 13, AWA, chief scientist P. Brehmer). Observations made during these cruises were described more explicitly in Ndoye (2016), Capet et al. (2017), and Machu et al. (2019). We supplemented these observations with data acquired during campaigns carried out in February (NANSEN; Voituriez & Chuchla, 1978) and August (CINECA, chief scientist A. Thiriot) 1973. For recent surveys (2012–2014), SBE 43 DO sensors (accuracy of $\pm 2\%$ of saturation) were calibrated prior to the survey and confronted with samples collected during the survey and analyzed by the Winkler method. For NANSEN and CINECA, samples were analyzed by the Winkler method using an iodometric titration with an amperometric endpoint to validate electrochemical DO concentrations for which the accuracy is $\sim 1.5 \mu\text{mol kg}^{-1}$ (e.g., Aminot & K erouel, 2004).

2.2.3. Wind Data

Due to failures in the Melax wind sensor, ancillary wind data are used. Wind data from the Dakar airport meteorological station (DWS; 14°44'N–17°28'W 27 m; 30 min interval; Figure 1) are used to cover the periods of failed measurements at the Melax buoy. The 1/4° ASCAT (Advanced Scatterometer) satellite daily wind stress product processed at CERSAT (<ftp://ftp.ifremer.fr/ifremer/cersat/products/gridded/MWF/L3/ASCAT/Daily/>) is also used to characterize synoptic variability. For the latter, we extracted the closest pixel to the Melax buoy from the gridded product.

2.2.4. MERCATOR Outputs

Outputs of the global ocean circulation model (PSY4V2) at 1/12° (~10 km) horizontal resolution (operated by MERCATOR-Ocean-International; Lellouche et al., 2013) are used to fill in gaps in the salinity and current time series (see Section 2.6). This model assimilates satellite altimetry, satellite sea surface temperature (SST) and in situ data (ARGO profilers) on a global scale. The model vertical grid has 50 vertical levels, and there are 15 levels near the Melax buoy (located at 30 m depth in PSY4V2's bathymetry). Vertical resolution ranges between 1 m at surface and 4 m at 30 m depth.

2.2.5. Modis SOM-NVA Chl-*a* Data

Chl-*a* data used in this study result from a specific processing of Level-1 Modis data due to Sahara dust in the region of study. The atmospheric correction has been improved by processing the data using a neural approach based on a Kohonen map in areas where absorbant aerosols dominate. The self-organizing map and neuro-variational approach (SOM-NVA) was initially developed to estimate the contribution of Sahara dust on ocean color data measured by the SeaWiFS sensor (Diouf et al., 2013). The algorithm was then adapted to MODIS-Aqua observations, MODIS, and SeaWiFS being two sensors with similar characteristics and the same standard atmospheric correction algorithm (Gordon & Wang, 1994). SOM-NVA data used here are level 2 (L2) daily data at ~4 km resolution over the southern part of the Canary Islands system. Data pixels are averaged over the shelf (from the coast to the 100 m isobath that references the edge of the shelf) from 14° to 14.75°N to produce a time series for the southern Senegal shelf.

2.3. Methodology

2.3.1. Time Filtering

Different filtering methods are applied to the time series. For seasonal and synoptic time scale analyses, surface wind, temperature, salinity, oxygen, and current observations are smoothed with a 7-day low-pass filter. A high-pass filter (10'-30h) is used for the analysis of HF variability. An index $S(t)$ illustrating the low-frequency modulation of HF oscillations ($x(t)$) is computed as the low-pass-filter of $x^2(t)$.

2.3.2. Wavelet Analysis

Wavelet spectra are useful to analyze localized variations (frequency) in the power (energy) of time series (Torrence & Compo, 1998). They provide information on the dominant frequencies of the signal and on the temporal modulations of the signal intensity at these frequencies. Coherence and phase spectra between temperature, salinity, and oxygen series are calculated. The coherence spectrum expresses the correlation and the phase shift between two time series at different frequencies and periods.

2.3.3. Upwelling Event Definition

To help study the synoptic/intraseasonal variability a criterion based on wind intensity and direction is applied to define what we call an upwelling event. Wind intensity and upwelling response (in terms of SST) are strongly related over the southern Senegalese shelf (Ndoye et al., 2014). The south-east orientation of the coast between Dakar and ~14°N (Figure 1) indicates that the north-west wind sector is theoretically optimal for the development of upwelling. However, the isobath around Melax being complex (see Figure 1), we used the criterion used by Ndoye et al. (2014) which depends only on the meridional wind. Upwelling favorable wind associated with upwelling events is defined by a meridional wind speed greater than 5.5 m s⁻¹ (wind stress >0.02 N m⁻²) oriented toward the south ($V < 0$), and the time window considered is 1 day.

2.3.4. Filling the Gaps in the Time Series

The observations at the Melax buoy present several periods with gaps in time series due to the malfunction of certain sensors. The passage of the cyclone Fred on August 30, 2015 (Dieng et al., 2019; Jenkins et al., 2017) damaged the wind sensor which led to a data gap between August 30 and mid-October of that year. Abnormal ADCP measurements were recorded during the periods from mid-June to the end of November 2015 and from mid-June to the end of July 2016 after the instrument capsized for an unknown reason. In order to fill these gaps, we used auxiliary ASCAT and DWS wind (see Section 2.2) and MERCATOR current data (see Section 2.2). To adjust time series and limit temporal inconsistencies, we used a regression method according to the following formula:

$$X_{\text{Melax}} = a x X_{\text{Auxiliary}} + b$$

where X is either the wind or the current. The coefficients a and b were calculated using a method of least squares to minimize the misfit between the measurements and the auxiliary data over a time period where both time series are available (Table 2). The high correlations we obtained between Melax and ASCAT wind stress, and Melax and MERCATOR currents provide support for an analysis of the continuous time series

Table 2
Regression Coefficient (a) and Bias (b), Determination (R^2) and Correlation (r) Coefficients Calculated by a Least-Squares Method Using Time Series of Wind Stress (Zonal and Meridional) Measured at Melax and From ASCAT From February 11 to August 25, 2015

| Parameters | | a | b | R^2 | r |
|------------|-----------------------------|------|-------|-------|------|
| Wind | $T_{\text{Melax/Ascat}}^x$ | 0.76 | 0.05 | 0.71 | 0.86 |
| | $T_{\text{Melax/Ascat}}^y$ | 0.90 | -0.04 | 0.72 | 0.85 |
| Velocity | $u_{\text{Melax/MERCATOR}}$ | 0.53 | 0.00 | 0.81 | 0.90 |
| | $v_{\text{Melax/MERCATOR}}$ | 0.96 | 0.03 | 0.81 | 0.90 |

Note. The second line corresponds to the calculation of the same coefficients between Melax and modeled currents from February 11, 2015 to June 10, 2015.

filled with model data, as we perform below. However, whenever appropriate auxiliary data are carefully distinguished from in situ observations or ignored (see Figure 2).

As a consequence of a drift of the salinity sensor, we chose to replace the salinity measured from mid-February 2016 to the end of April 2016 (when the CTD was replaced) with the modeled salinity of PSY4V2, whose variability closely resembles that of the Melax salinity observation during the cold period of 2015 (Figure S1). The new sensor installed at the end of April 2016 (see Table 1) shows an offset of 0.1 psu between PSY4V2 and observed salinity in May 2016. This offset is therefore added to the PSY4V2 series.

2.3.5. Apparent Oxygen Utilization

Apparent Oxygen Utilization (AOU) is the difference between DO solubility (DO_{SAT}), the DO concentration at saturation given the measured temperature, salinity and pressure, and DO_{MEAS} the measured DO concentration in the water ($AOU = DO_{\text{SAT}} - DO_{\text{MEAS}}$). Such quantity indicates when biological activity acts to change the ambient DO concentration. AOU is negative when DO concentration is supersaturated due to photosynthesis and positive in the case of respiration. AOU values are often low in shallow water systems because of their contact with the atmosphere, but elevated AOU values are possible in subsurface waters. In this study, we used the 28 m CTD temperature and salinity, and DO to compute AOU.

2.3.6. Estimation of Organic Matter Respiration Rates Using Surface Chl- a

We used the MODIS SOM-NVA surface Chl- a daily data to provide a rough estimation of the respiration rates between February 2015 and August 2016. We first retrieved time periods with successive daily measurements and estimated primary production rates in $\text{mgChl m}^{-2} \text{day}^{-1}$ (Figure S2) over a 10 m thick mixed layer (note that the mixed layer depth [MLD] varies between ~ 5 and 20 m [Figure 2d] thus a 10 m mean value is used for simplicity). With these production rates, using a C/Chl ratio of 1/50, an O/C ratio of 138/106 (Sarmiento & Gruber, 2006), and a seawater density of $1,028 \text{ kg m}^{-3}$, assuming steady state (i.e., production and total respiration of the produced organic matter compensate each other), we estimate respiration rates which are presented in the discussion of the biogeochemical effects on oxygen concentrations (see Section 4).

2.3.7. Estimation of Vertical Mixing Rates at Melax

We estimated DO supply by vertical mixing at Melax. As direct measurements of the vertical gradient of DO were not available, it was estimated based on the synchronous HF fluctuations of oxygen and temperature (T) at the depth of the DO sensor ($z_0 = 28 \text{ m}$). The vertical gradient is decomposed as follows: $\partial_z \text{DO} = \partial_T \text{DO} \cdot \partial_z T$. During periods of synchronous oscillations, we first determined the successive minimum (T_{min} , DO_{min}) and maximum (T_{max} , DO_{max}) values for both temperature and DO to compute $\partial_T \text{DO}$. The temperature difference ($T_{\text{max}} - T_{\text{min}}$) was then related to a depth range ($z_{\text{max}} - z_{\text{min}}$) using the vertical profile of temperature at Melax, allowing to compute $\partial_z T = (T_{\text{max}} - T_{\text{min}}) / (z_{\text{max}} - z_{\text{min}})$. In order to limit the impact of horizontal transport, we selected oscillations during periods of weak advection from the ADCP measurements. The values of $\partial_z \text{DO}$ associated with the different oscillation events are listed in Table S1. The diffusive flux was then computed as $F_{\text{diff}}(z = z_0) = K_z \partial_z \text{DO}$ using K_z estimations from the literature. Assuming no diffusive flux at the bottom ($z_b = 35 \text{ m}$), the ventilation of the bottom layer due to vertical mixing is: $\text{Diff}(\text{DO}) = [F_{\text{diff}}(z_0) - F_{\text{diff}}(z_b)] / (z_0 - z_b) = K_z \partial_z \text{DO} / (z_0 - z_b)$.

3. Results

3.1. Seasonal and Year-to-Year Variability

3.1.1. Description of Seasonal Fluctuations

Wind stress, current, temperature, salinity, Chl- a , and DO time series showed a marked seasonality (Figure 2). During the 2015 cold season (February–May), the meridional wind stress (T_y) was southward and its

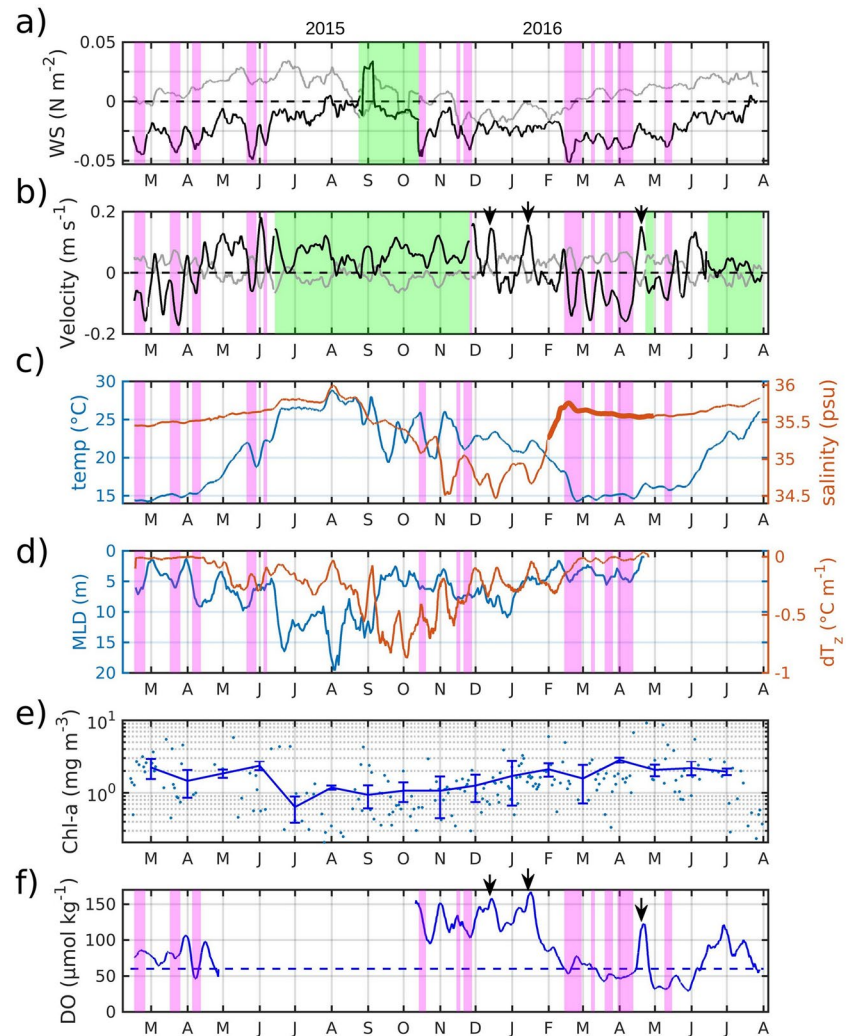


Figure 2. Low-pass (7 days) filtered time series for (a) surface wind stress (WS) (meridional [black] and zonal [gray] components, in N m^{-2}); (b) meridional (v ; black) and zonal (u ; gray) velocities (m s^{-1}); (c) temperature (blue, in $^{\circ}\text{C}$) and salinity (orange, in psu) measured at 28 m depth (7–8 m above sea floor) at Melax station from February 11, 2015 to August 1, 2016; (d) mixed layer depth (MLD; blue, in meters) and stratification index in the bottom layer (temperature gradient between 25 and 28 m, orange, in $^{\circ}\text{C m}^{-1}$); (e) daily (dots) and monthly (line) MODIS SOM-NVA chlorophyll concentration (in mgChl m^{-3}) from February 11, 2015 to August 1, 2016, averaged between 14° and 14.75°N and from the coast to the 100 m isobath, standard deviation is represented by the vertical line; (f) dissolved oxygen (DO, in $\mu\text{mol kg}^{-1}$) measured at 28 m depth. Pink shadings represent upwelling events defined by upwelling criterion (southward wind stronger than 5.5 m s^{-1} , see Section 2.3). The adjusted ASCAT wind stress and modeled current (see Section 2.3) at Melax (see pixels in Figure 1) are plotted and overlaid with green shading in (a and b), respectively. The adjusted model salinity (see Section 2.3) is plotted in (c) between February 2016 and the end of April 2016 (thick orange line). MLD is computed as $T(z = 1 \text{ m}) - T(z = \text{MLD}) = 0.2 \text{ }^{\circ}\text{C}$ (Montégut et al., 2004). The dotted blue line in (f) represents the hypoxia threshold set at $60 \mu\text{mol kg}^{-1}$. Black arrows (b and f) indicate periods of strong northward currents and DO concentration increase.

averages between 0.02 and 0.04 N m^{-2} (Figure 2a). During this upwelling period, near-bottom currents of $5\text{--}15 \text{ cm s}^{-1}$ were observed (Figure 2b). The relatively cold ($14 \text{ }^{\circ}\text{C}\text{--}16 \text{ }^{\circ}\text{C}$) and salty ($35.4\text{--}35.7 \text{ psu}$) near-bottom water was advected southward over the shelf. The MLD (see Figure 2's caption) during this period varied between ~ 1 and $\sim 10 \text{ m}$, increasing during wind bursts in mid-March and early April. Stratification (see Figure 2's caption) at 28 m depth was weak ($\sim 0.12 \text{ }^{\circ}\text{C m}^{-1}$, on average). Satellite data with intermittent coverage (Figure S2a) indicates that surface Chl- a concentration was around 2 mg m^{-3} (Figure 2e). DO concentration at 28 m depth varied between 50 and $100 \mu\text{mol kg}^{-1}$ (Figure 2f).

The transition period (mid-April–June 2015) from the cold season (upwelling) to the warm season was characterized by a reversal of the current from southward to northward in mid-April occurring ~2 months prior to a notable meridional wind stress weakening (after mid-June). This lag illustrates the importance of remote forcing (discussed in Section 4.3). Northward advection over the shelf was accompanied by a warming of the subsurface layer, with the temperature reaching 22 °C mid-May. Bottom-layer stratification increased with respect to the cold period, fluctuating between 0.13 °C and 0.3 °C m⁻¹.

In the warm season (June–September 2015), westerly winds prevailed and currents remained oriented northward. The surface layer reached its warmest (29 °C), saltiest (36 psu), and largest MLD (20 m) in August. Bottom-layer stratification increased between August and October with major synoptic fluctuations in early and late September. Salinity decreased gradually until mid-October as a consequence of heavy monsoon rainfall, both locally and regionally (low salinity water produced by rainfall occurring south of Senegal can be transported northward by the dominant coastal and slope currents at that period; Camara et al., 2015; Rebert, 1982). The surface Chl-*a* concentration decreased by 1.5 mg m⁻³ between June and July, reaching its minimum value (0.5 mg m⁻³). From August to November, the concentration of Chl-*a* varied at daily scale but was rather stable at monthly time scale (~1 mg m⁻³). Despite the lack of oxygen data during the warm period of interest, waters present over the shelf in summer are presumed to be relatively well-oxygenated (Brandt et al., 2015; Schütte et al., 2016; see also 2018 time series in Figure S3).

During the transition period to the cold season (mid-October 2015–January 2016) north-northeasterly winds dominated but currents remained oriented northward. Surface temperature (not shown) decreased rapidly likely due to intense cooling by air-sea fluxes, and the presence of fresh surface water that helps maintain barrier layers and temperature inversions (Faye et al., 2015). Hence, bottom water remained relatively warm (>21 °C) and stratified (>0.5 °C m⁻¹) but exhibited large fluctuations (±2 °C and ±0.4 °C m⁻¹) in October–November 2015. Salinity kept decreasing until early November when it reached a minimum (~34.5 psu) and then fluctuated strongly (±0.25 psu), due to the intermittent advection of relatively freshwater produced further south by monsoonal rainfall. The Chl-*a* concentration increased slightly but remained below 2 mg m⁻³. DO remained above 120 μmol kg⁻¹ over the entire period. In January 2016, the southward transport of colder, saltier, and oxygen-depleted water accompanied the return to the upwelling regime.

The temperature series at 35 m followed the minima of the temperature series at 28 m recorded at HF (Figure S4). The bottom temperature thus represented the low envelope of the temperatures recorded at 28 m. This indicates that the depth of 28 m is relevant to study the variability of the bottom layer. More specifically, the DO concentration measured at 28 m shall accurately represent bottom DO concentration of the bottom layer whenever the bottom and 28 m depth temperatures are equal.

3.1.2. Density-DO Relationship

The relationships between temperature, salinity, and oxygen exhibited a marked seasonality of the water masses in the bottom layer of the shelf (Figure 3). During the cold season (February–April 2015), bottom densities were greater than 25.8 kg m⁻³. The coldest temperatures (~14 °C) were associated with ~35.4–35.5 psu salinity and lower than 120 μmol kg⁻¹ DO concentrations (Figure 3a). One can notice the narrow spread of densities at that season.

The transition to the cold season (November 2015, Figure 3b) was characterized by a strong dispersion of DO concentrations (50–250 μmol kg⁻¹) and density values (21.5–25 kg m⁻³) with temperature and salinity in the range 19 °C–28 °C and 33.5–35.5 psu, respectively. At the start of the cold period in January, water cooled and became saltier ($T < 23.8$ °C; $S > 34.30$ psu in January 2016; Figure 3c) but remained above 19 °C and below 35.4 psu. During this period, oxygen concentrations varied widely (50–250 μmol kg⁻¹). Temperature and oxygen were positively correlated: the warmer the water, the more oxygenated it was (Figures 3b and 3c). In addition, a distinct water mass with salinity in the range 35.1–35.3 psu and DO below 100 μmol kg⁻¹ became prominent (Figure 3c). The transition to colder conditions continued through February 2016 and thereafter. During the first half of February, the water cooled down to ~17 °C and became denser (>24.5 kg m⁻³), while DO concentrations decreased down to ~50 μmol kg⁻¹ (Figure 3d). Subsequently (between mid-February and April 2016), the relationship between oxygen, temperature, and salinity changed drastically (Figure 3e). DO concentrations were then mostly below 100 μmol kg⁻¹ but lost their well-defined relationship with temperature and density (e.g., the highest measured DO concentrations were

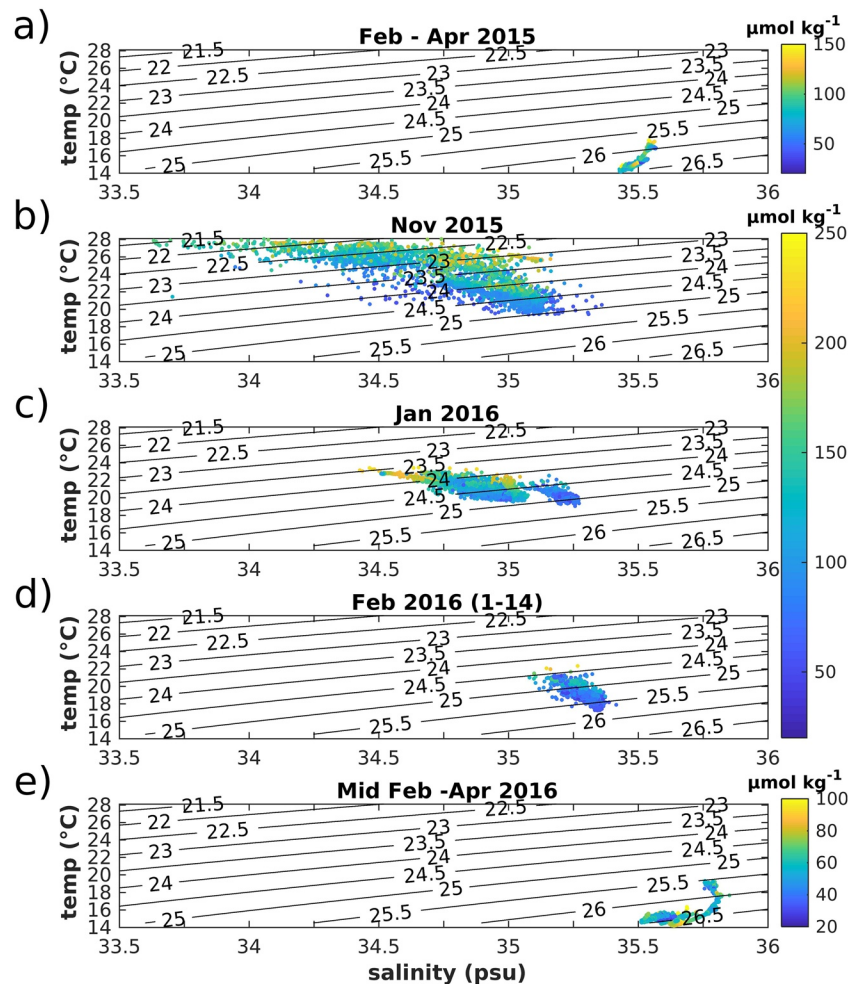


Figure 3. Temperature (°C)-salinity (psu)-dissolved oxygen ($\mu\text{mol kg}^{-1}$, color scale) diagrams of the water masses encountered on the shelf for the periods (a) February–April and (b) November 2015, (c) January, (d) 1–14 February and (e) from 15 February to the end of April 2016.

for the densest waters). The lowest DO concentrations ($20\text{--}50 \mu\text{mol kg}^{-1}$) were measured during this period of minimum density dispersion.

3.2. Intraseasonal Variability

Observations show a strong intraseasonal variability at time scales from a few days to a few weeks (Figure 2). In this subsection, we characterize this variability during the cold, the warm and the transition periods.

3.2.1. Upwelling Events in the Cold Season

On the south Senegalese shelf, upwelling is favored when the wind blows from the north/northwest (see Section 2.3). A dozen upwelling events (pink bands in Figure 2) were recorded during the cold periods of 2015 and 2016, including two stronger events ($\sim -0.05 \text{ N m}^{-2}$) in May 2015 and February 2016.

During the first cold season (February–May 2015), the meridional wind stress fluctuated between -0.01 and -0.045 N m^{-2} with a weakening trend throughout the season (Figure 2a). Each upwelling event was associated with an intensification of the southward subsurface current ($\sim -0.15 \text{ m s}^{-1}$; Figure 2b). The intense upwelling event in late May 2015 was associated with a relatively weak southward current ($\sim -0.05 \text{ m s}^{-1}$) interrupting a prolonged period (mid-April to end-of-May) of northward flow with speed $\sim 0.05\text{--}0.2 \text{ m s}^{-1}$.

Table 3

Maximum Cross-Correlation Between the Meridional Wind Stress (T_y), Temperature (T), Dissolved Oxygen, Zonal Velocity (u) and Meridional Velocity (v) at 28 m

| Cross-correlation | T_y -O ₂ | T -O ₂ | u -O ₂ | v -O ₂ | T_y - u | T_y - v |
|---------------------------|-----------------------|---------------------|---------------------|---------------------|-------------|-------------|
| Feb 12–Apr 23, 2015 | 0.76 (3) | 0.80 (0) | −0.88 (2) | 0.98 (1) | −0.86 (1) | 0.88 (1) |
| Nov 25, 2015–Feb 10, 2016 | 0.49 (1) | −0.72 (4) | −0.24 (0.5) | 0.48 (2) | −0.50 (0.5) | 0.48 (1) |
| Feb 12–Apr 23, 2016 | 0.78 (4.5) | 0.87 (6) | −0.80 (4) | 0.81 (4) | −0.62 (2) | 0.71 (2) |

Notes. Correlations are calculated for the 2015 and 2016 cold seasons and the transition period (25 November–10 February). Correlations are computed from the daily low-pass-filtered time series. The lag (in days) of the maximum correlation is given in brackets. All correlations are 95% significant.

During the cold season of 2016 (from mid-February to mid-May 2016), pulses of southward current occurred with intensities similar to those in 2015.

The bottom temperature shows relatively low intraseasonal variability during the two cold seasons (Figure 2c). Between mid-February and mid-April 2015, the temperatures ranged from 14 °C to 16 °C. Upwelling events generally caused only modest (e.g., −0.5 °C between mid- and late-March) or insignificant drops in temperature. In contrast, the bottom temperature dropped by ~3 °C in about 10 days during the late May 2015 upwelling event but this took place after a substantial bottom temperature warming in April and May. At the start of the 2016 cold season, the intense upwelling event of mid-February amplified the cooling trend initiated since mid-January. The temperature dropped to its absolute minimum for the entire measurement period (14.3 °C in mid-February 2016). Upwelling events between March and May 2016 caused small temperature fluctuations (~0.5 °C in mid-April and mid-May). The variations in salinity associated with upwelling events were extremely small in comparison with those of the warm season.

The DO response to upwelling wind fluctuations varied from event to event during the two cold seasons. The impact on DO of the first upwelling event of February 2015 appeared to be weak. The March 2015 event also had a limited effect on DO (~10 μmol kg^{−1} decrease). Changes of opposite sign and similar magnitude were associated with the relaxation events in late February and March 2015, and with those taking place over the entire 2016 cold season. Conversely, more intense DO fluctuations of magnitude ~50 μmol kg^{−1} or more were associated with the relaxation sequence in late March and early April 2015 and in April 2016. The April 2015 upwelling event was associated with rapid oxygen depletion and a period of hypoxia (DO < 60 μmol kg^{−1}) of ~10 days. Preparing for the interpretation of these time series, we now remark on some interesting subtleties. During the intense event of February 2016, the DO fluctuations remained weak but noticeably non-monotonic: DO decreased initially (while the flow was still oriented toward the north), then increased for a few days, and decreased again at the end of the event. Although the upwelling events between March and May 2016 were less intense than that of February 2016, the DO concentration appeared to be lower (<50 μmol kg^{−1}). During the 2016 cold season and until the end of May, concentrations were below the hypoxic threshold of 60 μmol kg^{−1}, except during a sudden reversal of the current toward the north (~0.15 m s^{−1}) around mid-April 2016.

We calculated the correlations between oxygen, wind and current to quantify the impact of upwelling events on DO concentration (Table 3). For the upwelling seasons 2015 and 2016, strong correlations are obtained between DO and the meridional current (2015: 0.98/1-day lag, 2016: 0.81/4-days lag) and to a lesser extent between DO and meridional wind stress (2015: 0.76/3-days lag, 2016: 0.78/4.5-days lag). Oxygen and zonal current are strongly anti-correlated (−0.88/2-days lag, −0.80/4-days lag, respectively), an eastward current being associated with a decrease in the DO concentration. To leading order, these correlations support the interpretation that advection toward the south-east is the dominant process to bring low-oxygen waters at Melax, in response to upwelling events. Given the dominant circulation pathways over the shelf (Ndoye et al., 2017), this low-oxygen water is presumably recently upwelled source water having undergone limited DO modifications. Note that correlations between DO and Chl-*a* could not be computed due to the numerous gaps in the Chl-*a* daily time series.

3.2.2. Intraseasonal Fluctuations During the Warm, Transition, and Early Upwelling Periods

Oxygen data during the warm season of 2015 are missing in our data set. DO observations made during the 2018 warm season (at a time when other Melax instruments were unfortunately out of the water) indicate

that large DO oscillations ($\sim 120 \mu\text{mol kg}^{-1}$; Figure S3) can also occur during this period and would deserve attention.

During the transition and early upwelling period (mid-October to January 2016), salinity and temperature showed strong fluctuation with the two variables being anti-correlated (Figure 2c). Water masses were relatively well-oxygenated ($\text{DO} > 100 \mu\text{mol kg}^{-1}$), with intraseasonal variations at ~ 15 days (Figure 2f) whose amplitude could reach $\sim \pm 50 \mu\text{mol kg}^{-1}$ (e.g., mid-October 2015). The more oxygenated and warm waters were of southern origin. They are associated with strong northward flow at Melax and presumably more broadly over the shelf (Faye et al., 2015; Kounta et al., 2018; Schütte et al., 2016). Although the correlations between current and oxygen are weaker (0.48, Table 3) during this period than during the upwelling season (Table 3), the hypothesis of oxygenation of the bottom layer in response to currents coming from the south is valid during the warm and the transition seasons.

3.2.3. Frequency Analysis

In order to investigate further the intraseasonal variability, global wavelet power spectra (GWPS) for DO, meridional wind stress, and zonal and meridional components of the current for the 2015 and 2016 cold seasons (February–April) and the transition period (October–January) were computed (Figure 4). For the cold season, significant peaks are observed at 7–10 and 16 days for DO (Figure 4a), 8–10 and 16 days for meridional wind stress (Figure 4b), and at 16 days for both current components (Figures 5c and 5d). This is in agreement with the observed relationship previously mentioned between upwelling events and south-east advection of oxygen-poor waters. Wind variability peaks were stronger in 2015, especially at 8 and 16 days. There was also a stronger variability of the current and the oxygen in 2015 than in 2016 at 16 days.

During the transition period, DO and meridional current showed significant variability at 16 days (Figures 4a–4d) whereas the GWPS energy of the meridional wind stress had a relative minimum at this frequency compared to energy at 8 and 32 days periods. This suggests the role of remote forcing of CTWs (Kounta et al., 2018; Polo et al., 2008) as a driver of DO fluctuations in this frequency band during that season. This mechanism could also be at work during the cold periods but be masked by the fact that local wind offshore of Senegal and remote winds further south responsible for the CTWs forcing (Kounta et al., 2018) undergo coherent intraseasonal fluctuations.

3.3. HF Variability

3.3.1. Diurnal Variability

The HF DO variance (see definition in Section 2.3) and the amplitude of DO fluctuations at short time scales can typically be respectively of the order of $3 (\mu\text{mol kg}^{-1})^2$ and $50 \mu\text{mol kg}^{-1}$ (Figures 4e and 5d). In this section, we examine the processes underlying this variability.

At daily time scales, water mass properties are weakly impacted by horizontal advection whose typical speeds are between 5 and 10 cm s^{-1} or roughly 5–10 km day^{-1} , the horizontal contrasts of temperature, salinity, or DO being relatively small over such distances. The biogeochemical source and sink terms for DO are also typically associated with longer time scales in the bottom layer (low primary production, relatively slow degradation of organic matter—see Machu et al., 2019). It is therefore expected that the dominant physical processes at this time scale will be vertical advection and diffusion.

During the cold season, spectral analysis shows diurnal variability that is significant for the wind stress (see Ndoye et al., 2014 for a description of the diurnal cycle during the upwelling season) and modest for currents and DO. The oxygen spectra exhibited a significant peak at 1 day only for the 2016 cold season (Figure 4e). The tidal signal was strongly dominated by the semidiurnal constituents as generally found on wide shelves (Clarke & Battisti, 1981; Rebert, 1982). The peaks for zonal and meridional currents were thus systematically below the significance level (Figures 4g and 4h). The variability of oxygen at the diurnal time scale, therefore, does not seem to be forced by horizontal advection. The diurnal wind and oxygen cycles (2016) were in phase quadrature (not shown), that is, an increase in oxygen concentration occurred about 6 h after the wind strengthening. In addition, AOU did not show evidence of net oxygen production by photosynthesis ($\text{AOU} > 0$) in the bottom layer during this period (Figure S5). These results suggest that in 2016, the oxygenation of the bottom layer could be produced by vertical mixing with the oxygen-rich surface layer.

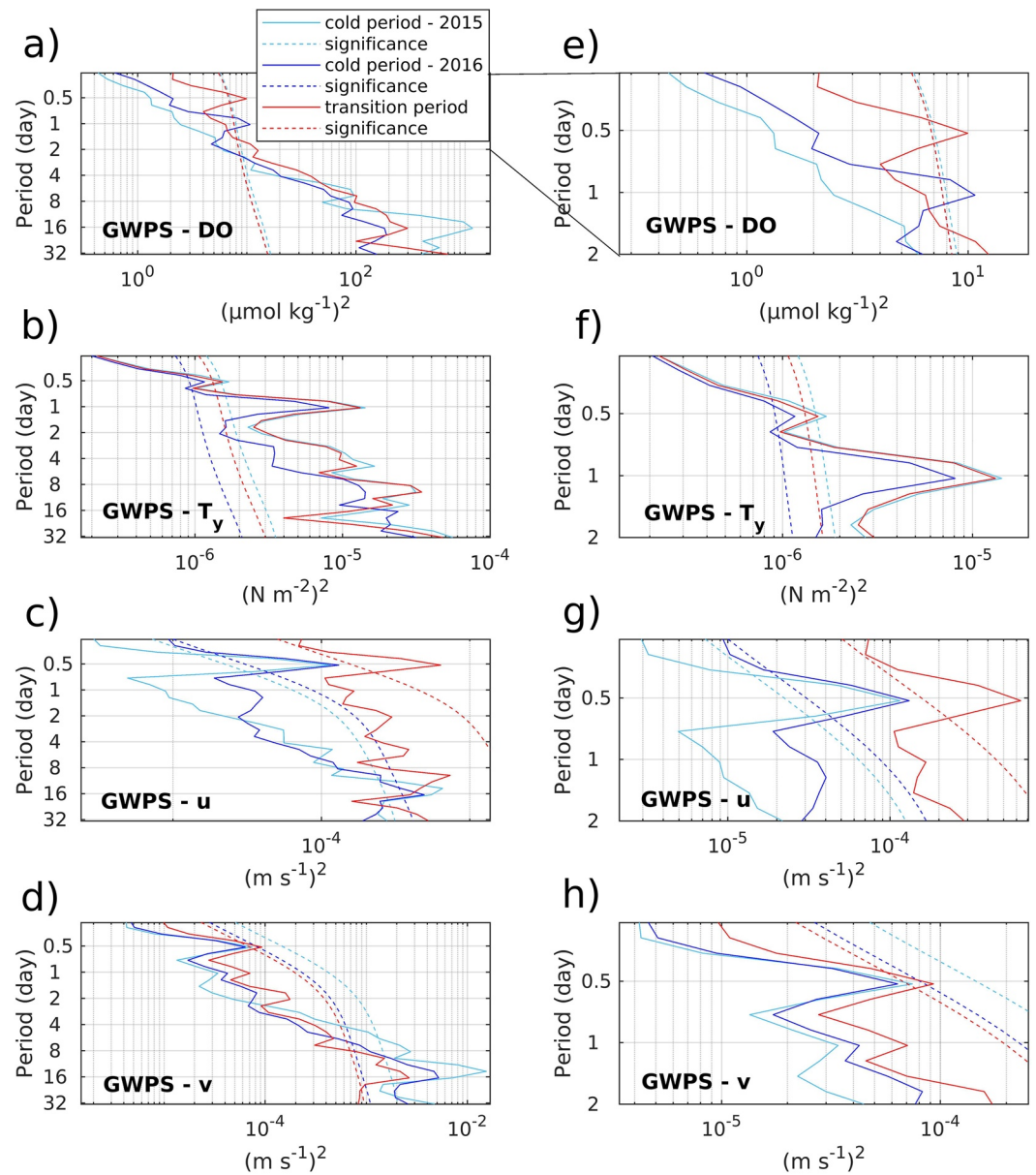


Figure 4. Global wavelet power spectra (GWPS) using Morlet's wavelet (i.e., Torrence & Campo, 1998) of (a) dissolved oxygen (DO), (b) meridional wind stress, (c) zonal and (d) meridional current velocities. (e–h) are zooms of panels (a–d) respectively for times scales shorter than 2 days. GWPS are shown in light blue (dark blue) for the cold periods of 2015 (2016) and in red for the transition from warm to the cold season. The dotted curves represent the significance thresholds of the corresponding spectra.

The absence of a diurnal peak for the oxygen spectra in the 2015 cold period despite an intense diurnal wind cycle however suggests that other factors than the wind, such as a diurnal oscillation of the oxycline or even horizontal advection of lateral DO gradients by inertial currents could also play a role. (Note again that the amplitude of the associated diurnal DO signals was relatively weak; see Figures 4e and 5d).

During the transition period, the diurnal variability of DO was not significant (Figure 4a) although that of the wind was of intensity comparable to that of the cold season 2015 (Figure 4b). During this period, AOU remained positive with values close to zero (Figure S5). Increased stratification of the water column during this warming period could inhibit vertical mixing forced by the diurnal variability of the wind (Figure 2d).

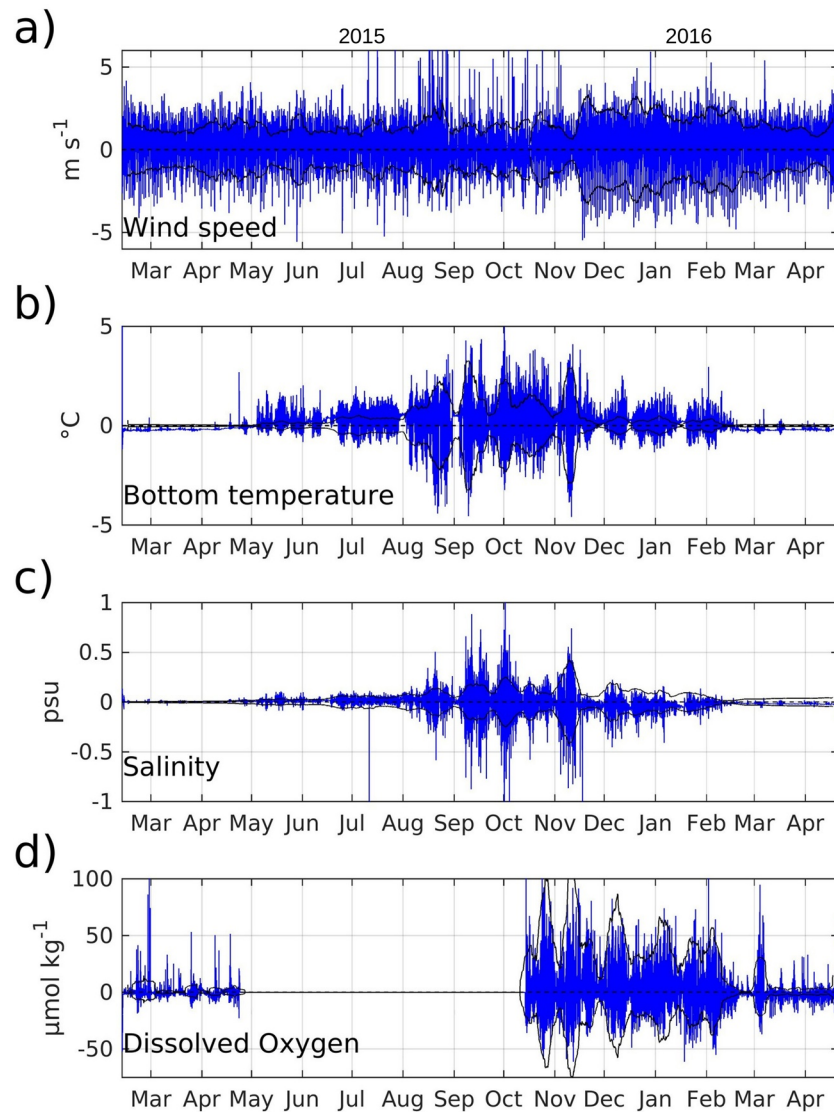


Figure 5. High pass filters (30 h) of (a) surface wind speed, (b) temperature, (c) salinity, and (d) dissolved oxygen concentration measured at 28 m at Melax from February 11, 2015 to April 26, 2016. The solid thin black lines represent the low-frequency modulations of the high-frequency variations of the different variables. DWS wind speed is used from the end of August to mid-October 2015 where wind data at Melax is missing (Section 2.3).

3.3.2. Semidiurnal Variability

Significant peaks of the variability of the zonal current at the scale of the semidiurnal tide (~ 12 h) were present during cold and transition periods (Figure 4g). The energy of the meridional current was systematically lower than that of the zonal current (Figure 4h), which is consistent with ADCP measurements made in 2013 (Capet et al., 2017) and regional modeling experiments taking tides into account (Ndoye, 2016). The semidiurnal variability of oxygen was significant only during the transition period (Figure 4e). The absence of a peak in cold periods suggests that the tide would affect the variability of oxygen only when the water column is sufficiently stratified (see Section 4).

3.3.3. Seasonal and Intraseasonal Modulation of High-Frequency Variability

The HF variability (HF; 10'–30h) of the tracers (temperature, salinity, and DO) shows a well-defined seasonality (Figure 5). During cold periods (February–April 2015 and mid-February–April 2016), the HF fluctuations in temperature and salinity were much less than during the rest of the year (Figures 5b and 5c).

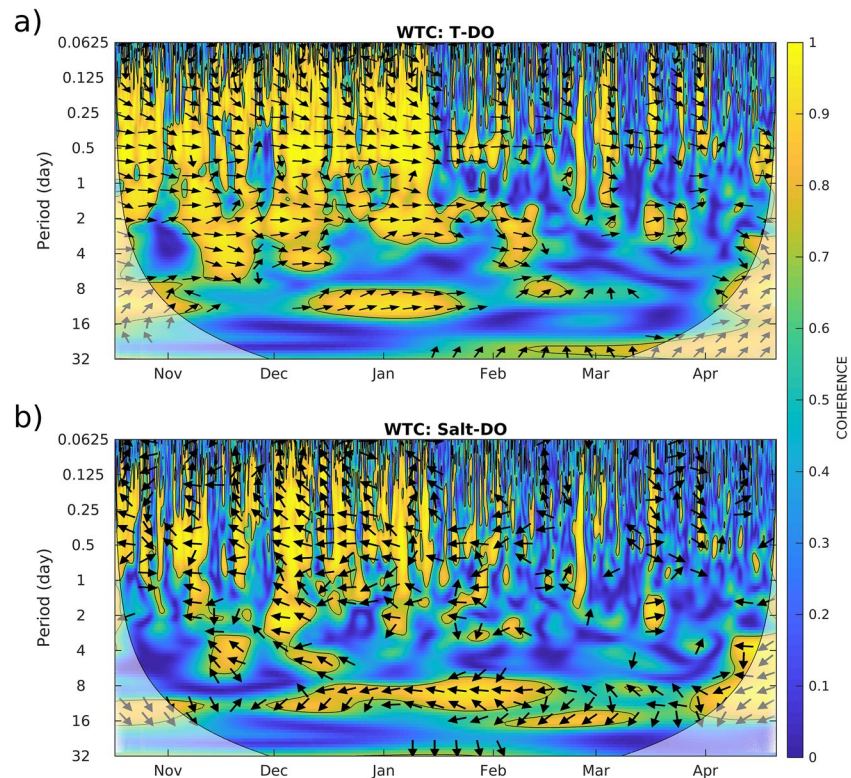


Figure 6. Wavelet Coherence (WTC) and phase spectrum (arrow, only zones where a coherence spectrum greater than 0.5 are represented) between (a) temperature and dissolved oxygen (DO), and (b) salinity and DO measured in the bottom layer between mid-October 2015 and end-of-April 2016. Black contours represent the 90% significance threshold based on 300 Monte Carlo simulations. The cone of influence is indicated at the edges where the power is undetermined because of the side effects. The arrows direction approaching $\pm 180^\circ$ indicates a phase opposition relation (maximum delay) and those close to 0° present a phase relation (minimum delay). The arrows close to $\pm 90^\circ$ show an offset relationship.

Larger amplitudes were recorded during the warm and transition periods (mid-August to mid-November 2015). During these periods, the temperature could vary by $\pm 5^\circ\text{C}$ around an average value within a few hours (for example at the beginning of October) while the salinity varied by up to ± 1 psu. The amplitude of the variations in temperature and salinity decreased but remained strong until the end of the transition period ($\pm 2^\circ\text{C}$ and ± 0.4 psu on December 10, 2015). HF oxygen variations were generally moderate in the cold season ($< \pm 50 \mu\text{mol kg}^{-1}$) but variations greater than $60 \mu\text{mol kg}^{-1}$ were however encountered in early March 2016 (Figure 5d). During the period mid-October to early February, the fluctuations in DO concentrations were around $\pm 75 \mu\text{mol kg}^{-1}$.

Amplitudes of HF fluctuations showed infra-monthly modulation, these amplitudes being low for example at the beginning of September 2015 after the passage of cyclone Fred (Dieng et al., 2019; Jenkins et al., 2017), end of November, mid-December, or mid-January 2016. The periods of maximum and minimum variability of the different tracers (temperature, salinity, and DO) are synchronous, but not correlated with those of the wind. Observations of the internal tide for 3 weeks during the 2013 cold season ~ 20 km south of Melax (Capet et al., 2017) help us to interpret the results obtained for the semidiurnal and HF fluctuations (see Section 4).

In order to better understand the HF variations of oxygen, we analyzed the consistency of its variations with those of temperature and salinity (Figure 6). The variations between temperature and oxygen were consistent and in phase during the transition period (mid-October 2015–mid-January 2016) at HF (< 12 h, Figure 6a). The variations in salinity and oxygen were also consistent but fluctuated in phase opposition during this period (Figure 6b). From mid-January 2016, the waters began to cool (Figure 2c) and the coherence spectrum changed. During the intensification of upwelling, oxygen and temperature were less cor-

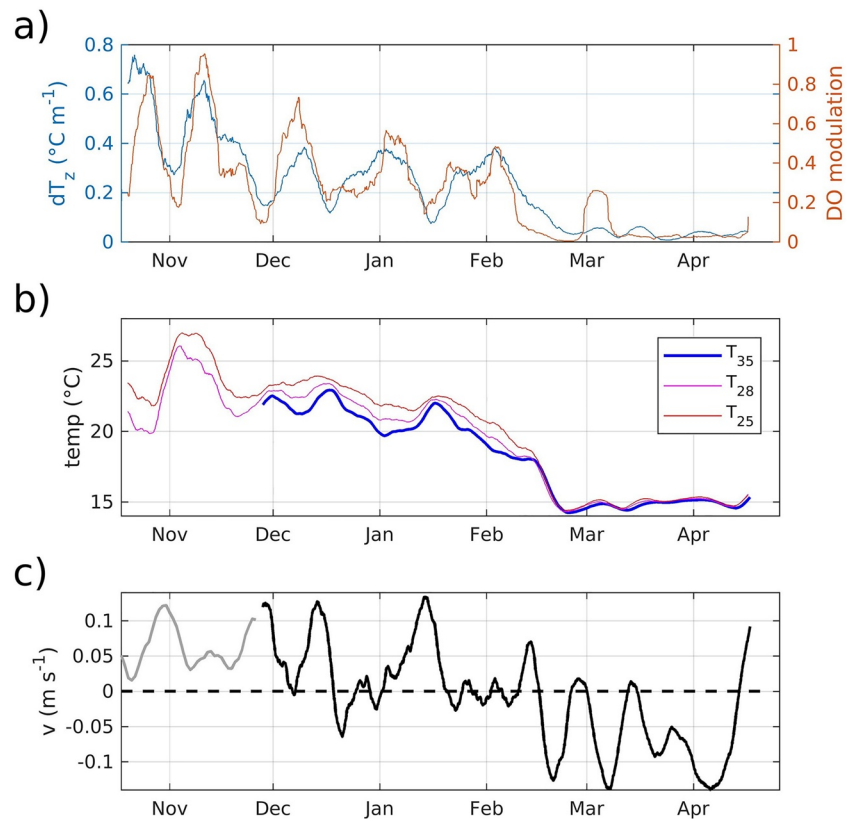


Figure 7. (a) Stratification index (blue, see Figure 2d) and low-frequency modulation of the high-frequency dissolved oxygen variations (orange); (b) Temperature variations at 25 m (red), 28 m (magenta), and 35 m (blue); (c) meridional current measured at 28 m (black) and simulated by the model (gray). The time series are low-pass (7 days) filtered.

related but coherent HF variations (>0.9) kept occurring over periods of a few days (Figure 6a). Note that oxygen and salinity varied in phase, as with temperature, during the events of mid-March and early April (Figure 6b).

Variations in stratification potentially play an important role in HF variations in DO. The oscillations in phase of oxygen and temperature (resp. salinity during the cold period) are consistent with vertical displacements of temperature (resp. salinity) and oxygen gradients at the depth of the DO sensor, associated with the passage of internal waves. The vertical temperature gradient is overwhelmingly positive, with warmer waters above colder waters (Figures 7a and 7b). The oxygen gradient is assumed to be predominantly positive as well, with oxygenated water above oxygen-depleted one. The phase opposition between salinity and DO is explained by the seasonal change of the vertical salinity gradient. It is negative (i.e., the water is less salty near the surface than near the bottom, not shown) during warm periods because of the monsoon precipitations and the presence of less salty water originating in the south. It becomes positive in cold periods when evaporation intensifies following intense northerly winds (Figure 2a), the surface layer becoming saltier than the bottom layer.

To explain the intraseasonal modulation in HF variability, an index measuring the intensity of the HF variations in oxygen is compared with other indices over the period November 2015 to April 2016 (Figure 7). The thermal stratification index near the bottom is obtained by calculating the temperature differences between 25 and 28 m. Salinity is not included in this diagnosis because observations are missing to calculate it in the bottom layer. However, its contribution to vertical stratification is generally negligible compared to that of temperature, the vertical gradients of salinity being relatively small (not shown). Low-frequency variations of the meridional current (Figure 7c) are also considered. There is a strong correlation (0.86) between the modulation of the HF oxygen variability and the stratification index (Figure 7a). This confirms our hypothesis: in the range of stratification intensities observed at Melax and more generally over the mid and outer

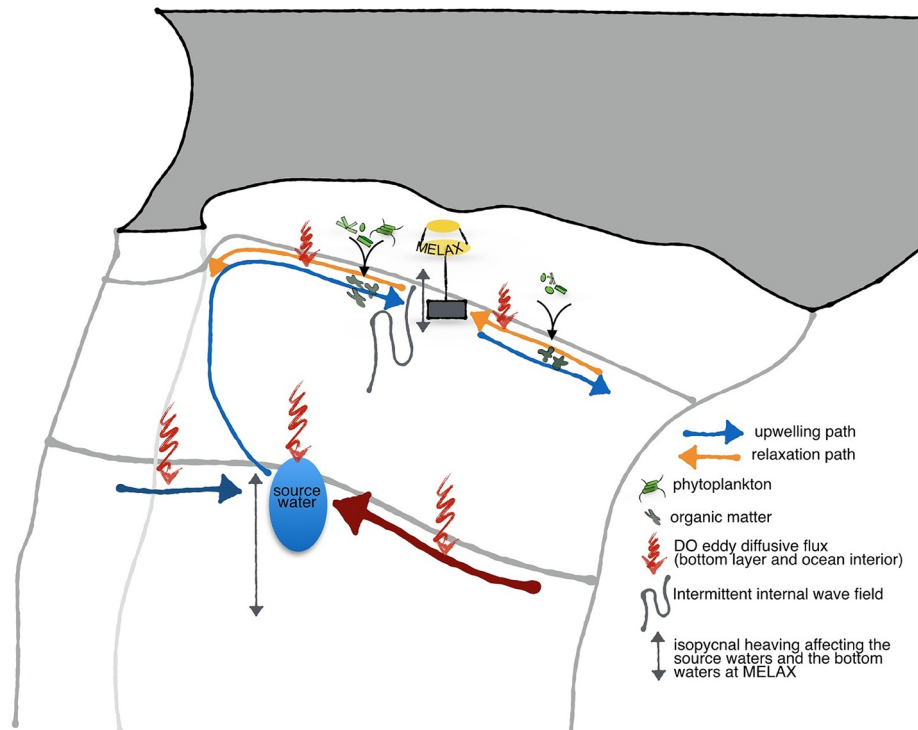


Figure 8. Schematic representation of the processes relevant to the dissolved oxygen (DO) dynamics over the southern Senegalese upwelling sector during the period January–February to April–May when equatorward circulation dominates over the shelf. Upwelling brings cold DO poor slope water onto the shelf following a relatively stable path that hugs the southern part of the Cape Verde peninsula. These source waters (which belong to the South Atlantic Central Water class) are drawn onto the shelf from a depth range that varies depending on local and remote conditions. They are typically brought to the Senegalese slope area by the West African boundary current but slope current variability and the existence of regional-scale DO gradients off West Africa implies that their properties can vary on synoptic and seasonal scales (see Section 4.3 for details). Vertical mixing can also impact source waters DO levels in high wind-low air-sea heat flux conditions in which the surface boundary layer turbulence reaches down to typical source water depths. Isopycnal heaving can also affect the properties of upwelling source waters. On their path to Melax, upwelling waters DO concentration can be modified by organic matter degradation and mixing. In relaxation conditions the shelf circulation tends to reverse to poleward and old upwelling waters previously advected southward may recirculate northward at Melax.

shelf, stronger (resp. weaker) stratification values near the bottom favor (resp. impede) the propagation of internal wave energy toward Melax, which yields larger (resp. lower) fluctuations of DO concentrations (for a given DO vertical gradient; in addition, stronger stratifications are likely to be associated with stronger DO vertical gradients).

HF variability of DO corresponds to a larger spread of bottom layer temperatures, the bottom temperature at 35 m exhibiting larger fluctuations compared to 25 and 28 m depth (Figure 7b). This indicates that stratification changes are mainly forced by changes in the bottom layer temperature. The phases with a reduced stratification and weak HF DO oscillations (e.g., in early and late November, as well as mid-December 2015) were associated with intense currents to the north (Figure 7c) which may induce frictional mixing and destroy the stratification, or transport less stratified waters from the southern shelf (Capet et al., 2017).

4. Discussion

The objective of this study is to characterize the variability of bottom oxygen on the Senegalese shelf and unravel the processes responsible for this variability. In the previous section, we described the variability of oxygen in the bottom layer over a wide range of time scales. We now turn in more details to the physical and biological processes controlling this variability. Our conceptual view of the circulation and DO dynamics over the southern Senegal sector is represented in Figure 8. We underscore the fact that the 3D nature

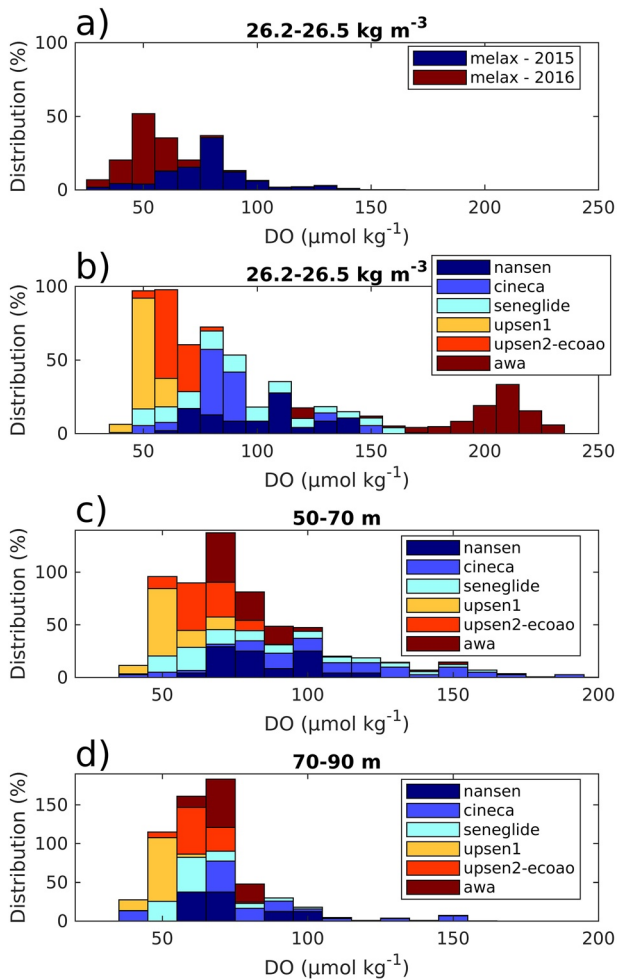


Figure 9. (a) Distribution of dissolved oxygen (DO) concentrations measured in the 26.2–26.5 kg m⁻³ density range during the upwelling seasons of 2015 and 2016 at Melax. Melax data are compared to (b) prior measurements collected during NANSEN (dark blue), CINECA (light blue), SENEGLIDE (sky blue) UPSEN1 (orange), UPSEN2-ECOAO (red), and AWA (brown) field experiments in the same density range. (c and d) indicate the DO concentrations from field experiments in two depth ranges. The locations where the data were taken are indicated in Figure 1. Except for the Melax data, all observations are from upper slope waters offshore of the shelf break.

of the circulation is important for this representation. It differs, in this regard, from previous 2D vertical conceptual models put forth to rationalize coastal DO dynamics in which alongshore invariance is assumed and across-shore flow is the dominant physical process (Harrison et al., 2016; Nam & Send, 2011).

4.1. Influence of Upwelling Source Water Properties at Melax

Our conceptual model of how slope waters reach Melax is based on recent high-resolution regional modeling experiments (Ndoye et al., 2017). The Eulerian and Lagrangian analyses of these numerical simulations suggest that upwelling source waters: are found in the depth range 50–100 m at the shelf break; follow a dominant upwelling pathway that is strongly constrained by the Cape Verde peninsula; and typically last 5–10 days from the shelf break to Melax. Hence, the relatively poorly oxygenated waters found on the shelf during the cold season are thought to be a consequence of the advection of low-oxygen source waters from the open ocean (Touré, 1983; Voituriez & Chuchla, 1978). At the surface, the main water mass encountered off West Africa is the oxygen-rich Tropical Surface Water (TSW). Below TSW, central waters are usually decomposed in an upper and a lower Central Water layer, the two layers being roughly delimited by the 26.8 kg m⁻³ isopycnal lying around 300 m depth (Elmoussaoui et al., 2005; Klenz et al., 2018; Peña-Izquierdo et al., 2015). Shelves are therefore under the influence of the upper Central Water (uCW) that flows northward along the shelf. Mainly composed of South Atlantic Central Water (SACW) off Senegal, the uCW mixes SACW and North Atlantic Central Water (NACW), the contribution of NACW increasing northward. Mean DO concentration of the uCW decreases northward presumably as a result of the degradation of the organic matter produced by the upwelling over the shelf (Klenz et al., 2018; Peña-Izquierdo et al., 2015).

The characteristics of these water masses vary on a wide range of time scales which, in turn, affects the characteristics of the waters found over the continental shelf during the upwelling season (e.g., see Connolly et al., 2010). It would be very useful to untangle the contributions of this type of DO variability at Melax as opposed to variability arising from near-bottom DO dynamics over the shelf (typically temporal changes in mixing and biological source/sink terms). We unfortunately have no precise knowledge of the density and depth range for the waters that were carried from the shelf break area to Melax's bottom layer during the 2015 and 2016 cold seasons (nor do we know the exact density-DO relationship as a function of time during these periods). These ranges vary at synoptic

and longer time scales under the influence of various interrelated processes: variability of the upper slope and outer shelf circulation due to mesoscale turbulence and coastal wave activity (see Section 4.3); modulation of the distribution of the Ekman return flow in the vertical due to stratification and alongshore pressure gradient changes (Jacox & Edwards, 2011; Lentz & Chapman, 2004; Marchesiello & Estrade, 2010); wind fluctuations; water mass transformation through mixing during the import journey to Melax.

To make progress on the correspondences (or lack thereof) between the variability in near-bottom water properties at Melax and that of offshore waters we: (a) take advantage of the shelf break water observations (depth > 100 m, Figure 1) made prior to 2015 during several research cruises (NANSEN, CINECA, UPSEN1, UPSEN2-ECOAO, and AWA, see Section 2) and a glider mission (SENEGLIDE); (b) consider three alternative choices for a fixed range of source water origin at the shelf break, that is, two distinct depth ranges (50–70 and 70–90 m) and the density range 26.2–26.5 kg m⁻³ (Figure 9). These three choices reflect our

perception of the uncertainty surrounding the origin of source water (see also Adams et al., 2013). Assuming a simplified 2D vertical Ekman circulation with negligible vertical mixing and alongshore pressure gradient effects, the source water origin would be a narrow depth range about 100 m, that is, at the isobath defining the shelf break offshore of Senegal. In reality, water situated higher up the water column must significantly contribute to upwelling, hence the two shallower depth ranges we retain. Over 90% of Melax near-bottom waters belong to the 26.2–26.5 kg m⁻³. This led to the third choice which is also a simplification of reality, given that source waters do not conserve their hydrological properties during their journey to Melax (Capet et al., 2017).

Consistent with the fact that source waters in the depth range 70–90 m are farther from the ocean surface than the ones in the depth range 50–70 m, DO values are less skewed toward high values and their variability is overall weaker for the deeper depth range (Figure 9). The same is true when the comparison is made with waters in the density range 26.2–26.5 kg m⁻³ which can be found at depths shallower than 70 m, owing to isopycnal heaving and/or air-sea cooling. Precisely, 75% of all observations fall between 45 and 95 μmol kg⁻¹ (the DO intervals to reach a similar 75% percentage are 45–100 μmol kg⁻¹ and 45–110 μmol kg⁻¹ for the shallow depth and density range of origin). Thus, even in the plausible situation where most of the near-bottom Melax water would originate from the 70–90 m depth range at the shelf break DO fluctuations due to source water variability shall be of the order of ±20 μmol kg⁻¹.

Therefore the differences in DO distribution at Melax between 2015 and 2016 could largely arise from differences in source water properties (Figure 9). Concomitant observations at Melax and the shelf break may be needed to gain additional insight. On the other hand, note that the lowest DO values found in 2016 and to a lesser extent 2015 have no correspondence in any of the shelf break DO profiles, which points to the role played by DO consumption (see Section 4.2).

In contrast, our knowledge of the shelf circulation patterns is very limited during the warm season when direct flow observations are not available (at Melax or elsewhere) and the origin of near-bottom waters passing through the mooring deduced from model simulations is variable and uncertain. During transition periods of weak upwelling dynamics and even more so during the warm season, we expect more effective decoupling between the properties of open ocean source waters and those of waters found at Melax, which have more time to be transformed through mixing and biogeochemical reactions, as examined next.

4.2. DO Variability at Melax Due to the Transformation of Upwelling Water Properties

4.2.1. Transformation by Biological Processes

Biological activity can impact DO concentrations on the shelf, acting either as a source (by photosynthesis) or a sink (by respiration of organic matter) of DO. DO production by subsurface primary production is unlikely to be important over the shelf during the upwelling season (Figure S5). Using satellite surface chlorophyll daily changes to estimate organic matter production (Figure S2), we computed approximate DO consumption or respiration rates. The respiration rates thus obtained ranged between 0 and 8 μmol kg⁻¹ day⁻¹ with an average around 2.6 ± 2.3 μmol kg⁻¹ day⁻¹ (resp. 1.7 ± 1.0 μmol kg⁻¹ day⁻¹) during the cold season of 2015 (resp. 2016). It is difficult to relate these rates to the phases of strong DO decrease observed at Melax (Figure 2f) because of the low spatial coverage and high number of data gaps (Figure S2). However, it would seem that biological processes could locally impact DO and induce phases of decrease of ~10–50 μmol kg⁻¹ in ~10 days.

We found that for the density range 26.2–26.5 kg m⁻³ (>90% of the near-bottom water encountered at Melax), the lowest concentrations measured on the shelf in 2015 and 2016 were lower than those of the source waters measured along the shelf break for several prior campaigns carried out during the cold season (Section 4.1, Figure 9). Using an approximate distance ($L \sim 100$ km) between the position of the source waters at the shelf break and the Melax station (Figures 1 and 8), and typical near-bottom horizontal velocities during an upwelling event ($V \sim 0.1$ m s⁻¹, Figure 2b), we estimate that the upwelling source waters at the shelf break would reach the Melax buoy in $T = L/V \sim 10$ days. Assuming that biological activity is solely responsible for the DO change during the transit of upwelling waters from the shelf break to Melax allows us to estimate a DO respiration-production rate $\tau = (DO_{\text{source}} - DO_{\text{Melax}})/T$ (negative τ would correspond to the situation where $DO_{\text{source}} < DO_{\text{Melax}}$).

Table 4

Respiration Rates ($\mu\text{mol kg}^{-1} \text{ day}^{-1}$) Calculated Using Mean DO Concentrations Measured at Melax in 2015 ($77.5 \pm 20.2 \mu\text{mol kg}^{-1}$) and in 2016 ($52.4 \pm 13.2 \mu\text{mol kg}^{-1}$) Under the Assumption That Water Masses Were Only Transformed by Biological Respiration From the Source Region to the Station (See Sections 2.3 and 4)

| | | NANSEN (1973) | SENEGLIDE (2011) | UPSEN1 (2012) | UPSEN2-ECOAO (2013) | AWA (2014) |
|--|------------------------------|---------------------------------|---------------------------------|---------------------------------|---------------------------------|----------------------------------|
| DO $\pm \sigma$ ($\mu\text{mol kg}^{-1}$) | 26.2–26.5 kg m^{-3} | 100.5 \pm 23.2 | 93.0 \pm 31.1 | 51.5 \pm 4.1 | 64.1 \pm 5.5 | 198.2 \pm 26.3 |
| | 50–70 m | 84.6 \pm 16.7 | 83.9 \pm 32.4 | 54.2 \pm 6.8 | 64.7 \pm 6.8 | 80.4 \pm 15.9 |
| | 70–90 m | 72.2 \pm 14.3 | 64.8 \pm 17.9 | 49.3 \pm 3.2 | 61.5 \pm 4.9 | 71.1 \pm 4.6 |
| Resp/Prod/Melax 2015 ($\mu\text{mol kg}^{-1} \text{ day}^{-1}$) | 26.2–26.5 kg m^{-3} | 2.3 \pm 3.1 | 1.5 \pm 3.8 | –2.6 \pm 2.1 | –1.3 \pm 2.1 | 12.1 \pm 3.3 |
| | 50–70 m | 0.7 \pm 2.6 | 0.6 \pm 3.5 | –2.3 \pm 1.5 | –1.3 \pm 1.5 | 0.3 \pm 2.6 |
| | 70–90 m | –0.5 \pm 2.5 | –1.3 \pm 2.7 | –5.8 \pm 2.0 | –1.6 \pm 2.1 | –0.6 \pm 2.1 |
| Resp/Prod/Melax 2016 ($\mu\text{mol kg}^{-1} \text{ day}^{-1}$) | 26.2–26.5 kg m^{-3} | 4.8 \pm 2.7 | 4.1 \pm 3.4 | –0.1 \pm 1.4 | 1.2 \pm 1.4 | 14.6 \pm 3.9 |
| | 50–70 m | 3.2 \pm 2.1 | 3.1 \pm 3.5 | 0.2 \pm 1.5 | 1.2 \pm 1.5 | 2.8 \pm 2.1 |
| | 70–90 m | 2.0 \pm 1.9 | 1.2 \pm 2.2 | –0.3 \pm 1.4 | 0.9 \pm 1.4 | 1.9 \pm 1.4 |

Notes. These respiration rates are calculated for source waters defined by a density range (26.2–26.5 kg m^{-3}) and depth ranges (50–70 m; 70–90 m). Source water DO concentrations are taken from prior NANSEN, UPSEN1, UPSEN2-ECOAO, SENEGLIDE, and AWA field experiments. Elevated respiration rates obtained when using AWA offshore DO values for the density range 26.2–26.5 kg m^{-3} shall be disregarded because waters in this density class are too close to the surface to feed the bottom layer at MELAX during this experiment carried out during unusually cold conditions. Positive values in bold indicate respiration rates calculated when the source water concentration is above than that observed at Melax.

Abbreviation: DO, dissolved oxygen.

We calculated several possible values of the respiration rate using the mean DO concentrations measured at Melax in 2015 ($77.5 \pm 20.2 \mu\text{mol kg}^{-1}$) and in 2016 ($52.4 \pm 13.2 \mu\text{mol kg}^{-1}$), and the mean source DO concentration measured for the different campaigns (Figure 1) in the layers defined by the density range 26.2–26.5 kg m^{-3} and by the depth 50–70 m and 70–90 m (Table 4). In this calculation, we do not consider CINECA which was conducted in 1973 during the summer season. If we exclude the high respiration rates obtained using the mean AWA DO concentration in the density range 26.2–26.5 kg m^{-3} , the respiration rates are between 0.2 and 4.8 $\mu\text{mol kg}^{-1} \text{ day}^{-1}$ (Table 4). These respiration rates are broadly consistent with the ones we obtained using Chl-*a* data and those measured off Senegal (3–5 $\mu\text{mol kg}^{-1} \text{ day}^{-1}$, Robinson et al., 2002) and on the Mauritanian shelf (0.75–1.5 $\mu\text{mol kg}^{-1} \text{ day}^{-1}$, Thomsen et al., 2019). Negative “respiration rates” suggest that other processes (e.g., physical) supply oxygen in the subsurface at rates that can become dominant over biological consumption (see below on vertical mixing).

The variability of respiration rates can be induced by the variability of primary production at intraseasonal to interannual time scales. Although few studies have measured primary production in EBUS, the existing ones show important variability of primary production in these regions (e.g., Arístegui & Harrison, 2002; Fernández et al., 2009; Jacob et al., 2018; Kahru et al., 2009; Kitidis et al., 2014; Lloyd, 1971; Mantyla et al., 1995; Mitchell-Innes & Walker, 1991).

4.2.2. Transformation by Surface Boundary Layer Turbulence During the Upwelling Season

Between February 17 and 20, 2016, very cold (14.3 °C) and salty (35.5–35.6 psu) waters underwent an increase in DO concentrations of $\sim 25 \mu\text{mol kg}^{-1}$ (Figure 2f) following a strong cooling at the surface and major reduction of the top-to-bottom water column stratification (from 2.5 °C to ~ 0.1 °C, not shown). Vanishing temperature difference between 25 and 35 m depth is visible in Figure 7. A situation with deep surface boundary layer (SBL) mixing was also observed over the continental shelf and slope during the AWA campaign. For example, salinity sections perpendicular to the coast exhibited high salinity structures (35–35.6 psu) between the surface and 80 m depth off the shelf (Figure not shown). DO concentrations of deep waters, mainly above 150 $\mu\text{mol kg}^{-1}$ during AWA (Figure 9), also suggest that denser and more oxygenated waters than usual (2012, 2013, 2015, 2016) were generated offshore and subsequently advected onto the shelf by upwelling.

More generally, surface cooling can be a very effective mechanism to oxygenate near-surface waters but it requires atmospheric conditions such that SBL turbulence reaches down to 30–40 m or more. Such conditions are not very frequent off southern Senegal because upwelling wind stress intensity rarely exceeds $0.04\text{--}0.05\text{ N m}^{-2}$ unlike off Central California where winds are twice as strong (e.g., Risien & Chelton, 2008) and hence ventilate subsurface layers more effectively during the upwelling season (Adams et al., 2013). Air-sea heat fluxes can help reinforce the turbulent destabilization of the water column. This would be frequent during the early part of the upwelling season, typically as long as the wind exhibits an offshore component and brings dry air from the land over the coastal ocean, thereby driving elevated outgoing latent heat fluxes. We therefore hypothesize that the modulation of SBL mixing on synoptic, seasonal, and inter-annual time scales is an intermittent contributor to near-bottom DO variability at Melax, through mixing of upwelling waters during their journey over the shelf and also through mixing of upper slope source waters, in extreme conditions (AWA campaign for instance). Note that the diurnal cycle of air-sea heat fluxes and of the wind (stronger winds in the evening and early part of the night; Ndoye et al., 2014) complicates this issue further by introducing a major source of SBL turbulence intermittency.

4.2.3. Transformation by Interior and Bottom Boundary Layer Turbulence

Subsurface turbulence mixing can also be produced by internal wave breaking and bottom friction. The progressive transformation of temperature and salinity properties of bottom waters as they traveled shoreward and southward during the upwelling phase of the UPSEN2/ECOAO experiments (Capet et al., 2017; their Figures 6 and 7) attests of the role played by these processes, at least over the outer shelf where SBL turbulence is generally insufficiently strong to reach the lower half of the water column. We expect DO modifications by interior and near-bottom shear-driven turbulence to be modest but less intermittent than those due to SBL turbulence. On the other hand, the interior stratification changes can greatly affect the strength and structure of the internal wavefield, with important implications for interior and near-bottom mixing (Capet et al., 2017) and, in turn, DO modifications between the shelf break and Melax. During the 2014 AWA cruise, circumstantial observations of energetic solibores (Figure not shown, see e.g., Walter et al., 2012, 2014 for some manifestations and implications along the US West Coast) were made in conditions where stratification was confined into the lower half of the water column. Subsurface mixing may exert a stronger influence on DO during the warm season when near-bottom waters presumably spend longer time periods over the shelf. However, the effect of mixing remains unable to erode the vertical gradient of DO near the bottom, as revealed by HF DO fluctuations that last until the new upwelling season (Figures 5d and 6).

Ideally we would like to estimate the DO Lagrangian input due to vertical mixing processes for water parcels which travel from the offshore source region to the bottom layer at Melax:

$$\text{Diff}(\text{DO})_{\text{off}}^{\text{Melax}} = \frac{1}{\Delta t} \int_{\text{off}}^{\text{Melax}} \partial_z (K_z \partial_z \text{DO})(x(t), y(t), z(t)) dt$$

where Δt (~ 10 days) is the time taken by fluid parcels to travel from the shelf break to Melax and K_z is the vertical diffusion coefficient for DO. Some averaging over a large number of parcel pathways would then need to be performed in order to obtain a mean contribution of mixing processes to DO supply between the shelf break and Melax bottom layer.

There are numerous practical data limitations and issues that prevent us from evaluating this diffusive contribution: 3D turbulence intermittency and the difficulty to measure K_z accurately (we have presently no microstructure data in the area; Capet et al., 2017); large vertical gradients of K_z and $\partial_z \text{DO}$ with opposite signs which is a major source of error in the calculation of the integral in equation above. We thus limit ourselves to providing rough estimates of the diffusive supply of DO in the bottom layer at Melax over different time intervals with a fixed value of K_z , based on the methodology described in Section 2. For moderate turbulence ($K_z = 10^{-4}\text{ m}^2\text{ s}^{-1}$) we find values of $\text{Diff}(\text{DO})$ ($0.1\text{--}19.1\text{ }\mu\text{mol kg}^{-1}\text{ day}^{-1}$, see Table S1) that are typically of the same order of magnitude as DO consumption derived under the assumption that diffusion plays a negligible role (see Table 4). Moderate turbulence would thus only modestly raise oxygen consumption estimates and perhaps explain why Melax near-bottom DO can sometimes be higher than in offshore source waters. Higher turbulence levels as have been observed near the bottom over some continental shelves

(e.g., $K_z \sim 10^{-3} \text{ m}^2 \text{ s}^{-1}$ in Villamana et al., 2017) would imply that source waters are subjected to much larger consumption rates than given in Table 4. Hence, large discrepancies would exist between the latter and estimates based on satellite-derived primary production (see previous subsection), which we tend to consider as relatively robust. Pending in situ measurements and high resolution modeling exercises aimed at estimating DO fluxes over the shelf with sufficient confidence, we thus provisionally assume that vertical mixing does not play a systematic leading-order role in the interior DO Lagrangian balance for upwelling source waters and shall remain at most commensurate with DO consumption, if only because we do observe hypoxic events.

4.3. DO Variability Due to Lateral and/or Vertical Advection Processes

In the previous section, we considered the contribution of irreversible or biogeochemical processes to the variability of DO at Melax. In the context where spatial DO contrasts exist, fluctuations of the horizontal and vertical velocity field can also produce DO variability at Melax through advection, as has been observed in other systems for a broad range of time scales (Monteiro et al., 2008; Nam & Send, 2011).

4.3.1. DO and Alongslope Current Variability

Alongslope current variability has two potentially important implications on near-bottom DO levels at Melax, through changes in source water properties. First, the regional distribution of DO over the WA upper slope is characterized by a poleward gradient that has been evidenced by Brandt et al. (2015) based on historic observations in the region. Although the DO field is heterogeneous at meso- and finer-scales (Kolodziejczyk et al., 2018; Schütte et al., 2016) we thus expect phases of predominantly poleward (resp. equatorward) boundary currents to bring source waters for the southern Senegal upwelling that are, on average more (resp. less) oxygenated. In this regard, the Senegal upwelling sector might differ from the Mauritania sector where the proximity of NACW to the north leads to increasing subsurface DO levels in conditions of sustained equatorward flow (Klenz et al., 2018; Peña-Izquierdo et al., 2015).

On the other hand, thermal wind balance implies that poleward (resp. equatorward) boundary currents over the upper slope are associated with a depressed (resp. uplifted) thermocline/oxycline. As the DO vertical gradient is oriented upward in the depth range where the source waters are drawn from, source waters from a similar depth range would be more (resp. less) oxygenated in case of a poleward (resp. equatorward) boundary current. Therefore two antagonistic effects on DO concentrations of source waters may result from subinertial variability in along-slope circulation. They are discussed in the sequence below.

The slope currents are subjected to both intraseasonal and seasonal variability (Faye et al., 2015; Klenz et al., 2018; Kounta et al., 2018; Polo et al., 2008). The latter is dominated by a semiannual cycle at the latitude of Senegal although observational evidence of this is limited (Busalacchi & Picaut, 1983; Kounta et al., 2018; Rossignol, 1973). The meridional gradient in subsurface DO is poorly constrained along the WA seaboard even at regional scale (e.g., see the paucity of DO observations in Brandt et al., 2015; e.g., their Figure 4). Based on the few observations reported in Brandt et al. (2015) and ignoring any possible bias due to unresolved temporal variability, we retain for the shallow oxygen minimum ($\sim 100 \text{ m}$) the following DO values for a back-of-the-envelope calculation: $\sim 50 \mu\text{mol kg}^{-1}$ at 18°N and $\sim 65 \mu\text{mol kg}^{-1}$ at 14°N which translates into $4 \mu\text{mol kg}^{-1}/100 \text{ km}$ for the DO lateral gradient at regional scale in the coastal waveguide. Intraseasonal flow anomalies of the order of $10\text{--}15 \text{ cm s}^{-1}$ over 15 days would thus lead to changes in DO $\sim 5\text{--}8 \mu\text{mol kg}^{-1}$. Using the meridional DO gradient calculated above on longer time scales is presumably irrelevant because eastern boundary undercurrents do not carry water coherently over hundreds of kilometers in the alongslope direction, owing to parallel flow instabilities, flow-topography interactions, and the resulting across-slope water exchanges (Barth et al., 2000; Durazo, 2015; Garfield et al., 1999). But DO fluctuations $\sim 10 \mu\text{mol kg}^{-1}$ or more are certainly plausible.

Vertical DO profiles exhibit a complex structure with strong gradients in the upper thermocline down to $\sim 100\text{--}120 \text{ m}$ depth, typically tens of $\mu\text{mol kg}^{-1}$ over a depth range of $20\text{--}30 \text{ m}$ (Figure S6). On seasonal as well as intraseasonal time scales isopycnal heaving can produce vertical displacements of the thermocline (and therefore of the oxycline) of tens of meters in amplitude (Kounta et al., 2018). The consequences in terms of upwelling source water DO depend on where their origin depth is positioned relative to the oxycline and DO minimum, and also on how this origin depth is affected by the flow perturbation/isopycnal

heaving (e.g., through alongshore pressure gradients and stratification anomalies (Jacox & Edwards, 2011; Lentz & Chapman, 2004; Marchesiello & Estrade, 2010). Examination of individual DO vertical gradients in source waters (Figure S6) suggests that DO variability could reach a few tens of $\mu\text{mol kg}^{-1}$ for typical thermocline displacements of 20 m or more (Klenz et al., 2018, their Figure 8; Kounta et al., 2018).

4.3.2. DO and Synoptic Variability of the Mid-Shelf Flow

A second category of advective driver of DO variability at Melax concerns alongshore flow over the mid-shelf. Mid-shelf circulation is obviously mostly parallel to isobaths (Figure 1). The two directions, poleward and equatorward, are equally important as visual inspection of Figure 1 reveals. Equatorward circulation tends to dominate during the cold season and this is consistent with the presence of a coastal upwelling jet being frequently in the vicinity of Melax. Note that wind relaxations during the early part of the upwelling season do not necessarily lead to flow reversals (Figures 2a and 2b).

The effect of synoptic flow reversals on DO is variable in magnitude and even in sign. Flow relaxations during the upwelling season can lead to an increase in DO by as much as $50 \mu\text{mol kg}^{-1}$ (April 2016, January 2016, June 2016), little change (early March 2016), or a decrease (early March 2015, April 2015) in DO concentration. Translated in terms of a DO meridional gradient at Melax (i.e., assuming that meridional advection is the sole process responsible for the changes at these scales), this hints at a more complex picture for the upwelling season than conveyed by Figure 8. Intuitively, we expected to see the manifestation of aging waters toward the south as the bottom waters contribute to the degradation of organic matter. However, oxygenation of shelf bottom waters through mixing may dominate over DO biological consumption in some instances. This would then induce an equatorward increase in DO consistent with the DO evolution observed at Melax during some relaxation periods, assuming that meridional advection is the dominant process. Possibly missing elements also include:

- The fact that mid-shelf phytoplankton production/biomass is itself modulated at synoptic time scales and is typically low during strong upwelling events (Lathuilière et al., 2008). In addition, the relatively intense equatorward flows associated with upwelling events imply that any phytoplankton bloom produced north of Melax has had limited time to age and sediment. Consequently, such events are not necessarily conducive to elevated DO consumption rates along southward Lagrangian pathways. This may be the reason why DO is less variable at certain times when the flow relaxes from equatorward to poleward (e.g., compare February 2015 and late March-April 2015).
- The fact that across-shore currents may play an important role because primary production and phytoplankton biomass have large across-shore gradients, particularly during the early and late part of the upwelling season (Demarcq, 2009). In Machu et al. (2019), it was conjectured that the anoxic event observed in 30 m of water just 20 km north of Melax was the result of offshore advection of more coastal waters subjected to high degradation rates.

4.3.3. Remote Forcing and Coastal Trapped Wave Activity

We finish with some general remarks about the shelf and slope current system off West Africa. Although substantial correlations exist between them, the variability of upwelling winds and alongshore currents exhibit important distinctions. For example, the intraseasonal oscillations of the meridional current are of comparable amplitude during the 2015 and 2016 upwelling seasons whereas the amplitude of wind fluctuations is significantly lower in 2016. The flow response to individual synoptic wind fluctuations is also quite variable. This variability is presumably related to intraseasonal CTWs propagating along the WA coasts (Diakhaté et al., 2016; Kounta et al., 2018; Polo et al., 2008). These waves can be generated south of Senegal, as far as from the Gulf of Guinea (remote forcing from the equatorial strip has been shown to have a limited effect off Senegal; Kounta et al., 2018; Polo et al., 2008), and then propagate along the coasts of West Africa. CTWs can modulate the alongshore currents over the Senegalese continental slope and shelf, irrespective of the local wind evolution. Note though that wind fluctuations tend to be coherent at regional scale so that local and remote wind effects frequently reinforce each other in driving coastal wave activity and circulation changes. The shelf response to remote forcing is a delicate issue (Brink, 1991) on which we plan to make progress numerically, given the potential implications for coastal DO dynamics as found in other regions (Brüchert et al., 2006; Espinoza-Morriberón et al., 2019; Gutiérrez et al., 2008; Naqvi et al., 2006).

5. Conclusion and Perspectives

In the bottom layer observed at the Melax station located on the wide and shallow shelf of the south Senegalese shelf, we studied the role of the main physical processes on the variability of DO for different time scales ranging from a few tens of minutes (internal tidal waves) to the season.

During the upwelling season, the winds are from the north/northwest, and the currents are mostly southward. Upwelling triggers phytoplankton blooms in the surface layer and brings cold, salty waters with DO concentrations close to the hypoxic threshold. The properties of the water masses encountered at Melax are in agreement with the hypothesis that these waters originate at the shelf edge. These properties vary according to the circulation along the slope which conditions the water masses in presence and displace density and oxygen properties vertically and horizontally. Once they are over the shelf, upwelling source waters are subjected to DO respiration at rates broadly consistent with the evolution of DO concentrations between the source zone and the mid-shelf mooring where near-bottom mooring is being monitored. Upwelling wind relaxation events associated with current reversals (from south to north) significantly modify the temperature, salinity, and DO properties at the mooring. Some intense SBL mixing events can reach down to appropriate depths and oxygenate near-bottom shelf waters as well as offshore source waters which have major but temporary consequences on DO distribution.

The monsoon season is characterized by weak westerly winds and northward currents that dominate. The waters of the bottom layer are 10 °C–15 °C warmer, their salinity decreases during the season and they are more oxygenated. The slower dynamics of this period leads to a stronger decoupling between the properties of the waters observed at Melax and those of the source waters. As this season is marked by much higher retention of water masses on the shelf (e.g., Mbaye et al., 2015), the shelf waters have more time to be transformed by mixing or biogeochemical reactions before they are returned offshore. During the long transition period between the warm season and the new upwelling season, northerly winds re-establish themselves while the currents remain predominantly northward (Figure 1). This situation is associated with a stratification that strengthens near the bottom layer. This stratification seems to inhibit the vertical mixing that could result from the diurnal wind cycle and induces HF variability in temperature, salinity, and DO. This variability is associated with internal waves generated by tides. The mixing induced by bottom friction and internal waves must be sufficiently modest to not erode the ubiquitous near-bottom vertical DO gradients observed over the mid-shelf. Finally, CTWs constitute a distant forcing that can act year-round, impacting both shelf waters and source regions.

Despite a limited understanding of biological processes and the limited length of our time series, one can wonder about the long-term variations in the oxygenation of the Senegalese shelf. One of the identified impacts of climate change in West Africa is the reduction (of the order of 10%–15% for RCP8.5 scenarios) of winds favorable to upwelling during the cold season (Soares et al., 2019; Sylla et al., 2019). A (slight) decrease in upwelling intensity superimposed on global warming is thus projected. Although it is difficult to anticipate the consequences on DO, a warming would alter oxygen air-sea transfer and thus reduce DO concentrations in surface layers, but also increase stratification and reduce mixing, both resulting in the deoxygenation of subsurface layers. Interestingly, the lowest DO concentrations measured off Mauritania occurred in summer when the stratification is maximum and hinders ocean interior ventilation through diffusive fluxes (Klenz et al., 2018). More observations and long-term temporal monitoring, as well as regional modeling experiments coupling physical and biogeochemical processes, will be necessary to better understand the potential effects of climate change on the evolution of oxygen and its impacts on marine resources on the Senegalese shelf.

Data Availability Statement

The readers can access the data supporting the analysis and conclusions here: <https://doi.org/10.5281/zenodo.4095435>.

Acknowledgments

A. W. Tall was supported for this study by an ARTS scholarship from IRD (Institut de Recherche pour le Développement) and by a SCAC scholarship from the French Embassy in Senegal. The French National Research Agency (ANR) partly funded this research (SOLAB project; grant ANR-18-CE32-0009). The authors also acknowledge support from the Laboratoire Mixte International ECLAIRS2 and from the French national program LEFE-GMMC (SENOX) and LEFE-CYBER-EC2CO (CENTRAL). The authors thank A. T. Gaye for his constant support to this work. Global ocean model outputs were provided from the Copernicus Marine Environment Monitoring Service (CMEMS, <https://marine.copernicus.eu/>).

References

Adams, K. A., Barth, J. A., & Chan, F. (2013). Temporal variability of near-bottom dissolved oxygen during upwelling off central Oregon. *Journal of Geophysical Research: Oceans*, 118(10), 4839–4854. <https://doi.org/10.1002/jgrc.20361>

Aminot, A., & Kérouel, R. (2004). *Hydrologie des écosystèmes marins: Paramètres et analyses*. Editions Quae.

Aristegui, J., & Harrison, W. (2002). Decoupling of primary production and community respiration in the ocean: Implications for regional carbon studies. *Aquatic Microbial Ecology*, 29(2), 199–209. <https://doi.org/10.3354/ame029199>

Barth, J. A., Pierce, S. D., & Smith, R. L. (2000). A separating coastal upwelling jet at Cape Blanco, Oregon and its connection to the California Current System. *Deep-Sea Research Part II: Topical Studies in Oceanography*, 47(5), 783–810. [https://doi.org/10.1016/S0967-0645\(99\)00127-7](https://doi.org/10.1016/S0967-0645(99)00127-7)

Brandt, P., Bange, H. W., Banyte, D., Dengler, M., Didwischus, S.-H., Fischer, T., et al. (2015). On the role of circulation and mixing in the ventilation of oxygen minimum zones with a focus on the eastern tropical North Atlantic. *Biogeosciences*, 12(2), 489–512. <https://doi.org/10.5194/bg-12-489-2015>

Breitburg, D., Levin, L. A., Oschlies, A., Grégoire, M., Chavez, F. P., Conley, D. J., et al. (2018). Declining oxygen in the global ocean and coastal waters. *Science*, 359(6371), eaam7240. <https://doi.org/10.1126/science.aam7240>

Brink, K. H. (1991). Coastal-trapped waves and wind-driven currents over the continental shelf. *Annual Review of Fluid Mechanics*, 23(1), 389–412. <https://doi.org/10.1146/annurev.fl.23.010191.002133>

Brüchert, V., Currie, B., Peard, K. R., Lass, U., Endler, R., Dübecke, A., et al. (2006). Biogeochemical and physical control on shelf anoxia and water column hydrogen sulphide in the Benguela coastal upwelling system off Namibia. In L. N. Neretin (Ed.), *Past and present water column anoxia* (pp. 161–193). Springer Netherlands. https://doi.org/10.1007/1-4020-4297-3_07

Busalacchi, A. J., & Picaut, J. (1983). Seasonal variability from a model of the tropical Atlantic Ocean. *Journal of Physical Oceanography*, 13(9), 1564–1588. [https://doi.org/10.1175/1520-0485\(1983\)013<1564:SVFAMO>2.0.CO;2](https://doi.org/10.1175/1520-0485(1983)013<1564:SVFAMO>2.0.CO;2)

Camara, I., Kolodziejczyk, N., Mignot, J., Lazar, A., & Gaye, A. T. (2015). On the seasonal variations of salinity of the tropical Atlantic mixed layer. *Journal of Geophysical Research: Oceans*, 120(6), 4441–4462. <https://doi.org/10.1002/2015JC010865>

Capet, X., Estrade, P., Machu, E., Ndoye, S., Grelet, J., Lazar, A., et al. (2017). On the Dynamics of the southern Senegal upwelling center: Observed variability from synoptic to superinertial scales. *Journal of Physical Oceanography*, 47(1), 155–180. <https://doi.org/10.1175/JPO-D-15-0247.1>

Chapman, P., & Shannon, L. V. (1985). The Benguela ecosystem. II: Chemistry and related processes. *Oceanography and Marine Biology*, 23, 183–251.

Checkley, D. M., & Barth, J. A. (2009). Patterns and processes in the California Current System. *Progress in Oceanography*, 83(1), 49–64. <https://doi.org/10.1016/j.pocean.2009.07.028>

Clarke, A. J., & Battisti, D. S. (1981). The effect of continental shelves on tides. *Deep-Sea Research Part A. Oceanographic Research Papers*, 28(7), 665–682. [https://doi.org/10.1016/0198-0149\(81\)90128-x](https://doi.org/10.1016/0198-0149(81)90128-x)

Conley, D. J., Carstensen, J., Ærtebjerg, G., Christensen, P. B., Dalsgaard, T., Hansen, J. L. S., & Josefson, A. B. (2007). Long-term changes and impacts of hypoxia in Danish coastal waters. *Ecological Applications*, 17(sp5), S165–S184. <https://doi.org/10.1890/05-0766.1>

Connolly, T. P., Hickey, B. M., Geier, S. L., & Cochlan, W. P. (2010). Processes influencing seasonal hypoxia in the northern California Current System. *Journal of Geophysical Research*, 115(C3). <https://doi.org/10.1029/2009JC005283>

Demarcq, H. (2009). Trends in primary production, sea surface temperature and wind in upwelling systems (1998–2007). *Progress in Oceanography*, 83(1), 376–385. <https://doi.org/10.1016/j.pocean.2009.07.022>

Diakhaté, M., de Coëtlogon, G., Lazar, A., Wade, M., & Gaye, A. T. (2016). Intraseasonal variability of tropical Atlantic sea-surface temperature: Air-sea interaction over upwelling fronts. *Quarterly Journal of the Royal Meteorological Society*, 142(694), 372–386. <https://doi.org/10.1002/qj.2657>

Dieng, A. L., Ndoye, S., Jenkins, G. S., Sall, S. M., & Gaye, A. T. (2019). *Estimating zonal Ekman transport along coastal Senegal during passage of Hurricane Fred (2015) from August 30 to 31, 2015*. <https://doi.org/10.20944/preprints201911.0125.v1>

Diouf, D., Niang, A., Brajard, J., Crepon, M., & Thiria, S. (2013). Retrieving aerosol characteristics and sea-surface chlorophyll from satellite ocean color multi-spectral sensors using a neural-variational method. *Remote Sensing of Environment*, 130, 74–86. <https://doi.org/10.1016/j.rse.2012.11.002>

Durazo, R. (2015). Seasonality of the transitional region of the California Current System off Baja California. *Journal of Geophysical Research: Oceans*, 120(2), 1173–1196. <https://doi.org/10.1002/2014JC010405>

Elmoussaoui, A., Arhan, M., & Treguier, A. M. (2005). Model-inferred upper ocean circulation in the eastern tropics of the North Atlantic. *Deep-Sea Research Part I: Oceanographic Research Papers*, 52(7), 1093–1120. <https://doi.org/10.1016/j.dsr.2005.01.010>

Espinoza-Morriberón, D., Echevin, V., Colas, F., Tam, J., Gutierrez, D., Graco, M., et al. (2019). Oxygen variability during ENSO in the tropical South Eastern Pacific. *Frontiers in Marine Science*, 5. <https://doi.org/10.3389/fmars.2018.00526>

Faye, S., Lazar, A., Sow, B. A., & Gaye, A. T. (2015). A model study of the seasonality of sea surface temperature and circulation in the Atlantic North-Eastern Tropical Upwelling System. *Frontiers in Physiology*, 3. <https://doi.org/10.3389/fphys.2015.00076>

Fernández, C., Fariás, L., & Alcaman, M. E. (2009). Primary production and nitrogen regeneration processes in surface waters of the Peruvian upwelling system. *Progress in Oceanography*, 83(1), 159–168. <https://doi.org/10.1016/j.pocean.2009.07.010>

Garau, B., Ruiz, S., Zhang, W. G., Pascual, A., Heslop, E., Kerfoot, J., & Tintoré, J. (2011). Thermal lag correction on Slocum CTD glider data. *Journal of Atmospheric and Oceanic Technology*, 28(9), 1065–1071. <https://doi.org/10.1175/JTECH-D-10-05030.1>

Garfield, N., Collins, C. A., Paquette, R. G., & Carter, E. (1999). Lagrangian exploration of the California undercurrent, 1992–95. *Journal of Physical Oceanography*, 29(4), 560–583. [https://doi.org/10.1175/1520-0485\(1999\)029<0560:LEOTCU>2.0.CO;2](https://doi.org/10.1175/1520-0485(1999)029<0560:LEOTCU>2.0.CO;2)

Gilbert, D., Rabalais, N. N., Diaz, R. J., & Zhang, J. (2010). Evidence for greater oxygen decline rates in the coastal ocean than in the open ocean. *Biogeosciences*, 7(7), 2283–2296. <https://doi.org/10.5194/bg-7-2283-2010>

Gordon, H. R., & Wang, M. (1994). Retrieval of water-leaving radiance and aerosol optical thickness over the oceans with SeaWiFS: A preliminary algorithm. *Applied Optics*, 33(3), 443–452. <https://doi.org/10.1364/AO.33.000443>

Gutiérrez, D., Enriquez, E., Purca, S., Quipúzcoa, L., Marquina, R., Flores, G., & Graco, M. (2008). Oxygenation episodes on the continental shelf of central Peru: Remote forcing and benthic ecosystem response. *Progress in Oceanography*, 79(2), 177–189. <https://doi.org/10.1016/j.pocean.2008.10.025>

Harrison, C. S., Hales, B., Siedlecki, S., & Samelson, R. M. (2016). Potential and timescales for oxygen depletion in coastal upwelling systems: A box-model analysis. *Journal of Geophysical Research: Oceans*, 121(5), 3202–3227. <https://doi.org/10.1002/2015JC011328>

- Jacob, B. G., Tapia, F. J., Quiñones, R. A., Montes, R., Sobarzo, M., Schneider, W., et al. (2018). Major changes in diatom abundance, productivity, and net community metabolism in a windier and dryer coastal climate in the southern Humboldt Current. *Progress in Oceanography*, 168, 196–209. <https://doi.org/10.1016/j.pocean.2018.10.001>
- Jacox, M. G., & Edwards, C. A. (2011). Effects of stratification and shelf slope on nutrient supply in coastal upwelling regions. *Journal of Geophysical Research*, 116(C3). <https://doi.org/10.1029/2010JC006547>
- Jenkins, G. S., Brito, E., Soares, E., Chiao, S., Lima, J. P., Tavares, B., et al. (2017). Hurricane Fred (2015): Cape Verde's first hurricane in modern times: Observations, impacts, and lessons learned. *Bulletin of the American Meteorological Society*, 98(12), 2603–2618. <https://doi.org/10.1175/BAMS-D-16-0222.1>
- Kahru, M., Kudela, R., Manzano-Sarabia, M., & Mitchell, B. G. (2009). Trends in primary production in the California Current detected with satellite data. *Journal of Geophysical Research*, 114(C2). <https://doi.org/10.1029/2008JC004979>
- Kitidis, V., Tilstone, G. H., Serret, P., Smyth, T. J., Torres, R., & Robinson, C. (2014). Oxygen photolysis in the Mauritanian upwelling: Implications for net community production. *Limnology & Oceanography*, 59(2), 299–310. <https://doi.org/10.4319/lo.2014.59.2.0299>
- Klenz, T., Dengler, M., & Brandt, P. (2018). Seasonal variability of the Mauritanian current and hydrography at 18°N. *Journal of Geophysical Research: Oceans*, 123(11), 8122–8137. <https://doi.org/10.1029/2018JC014264>
- Kolodziejczyk, N., Testor, P., Lazar, A., Echevin, V., Krahnmann, G., Chaigneau, A., et al. (2018). Subsurface fine-scale patterns in an anticyclonic eddy off Cap-Vert Peninsula observed from glider measurements. *Journal of Geophysical Research: Oceans*, 123(9), 6312–6329. <https://doi.org/10.1029/2018JC014135>
- Kounta, L., Capet, X., Jouanno, J., Kolodziejczyk, N., Sow, B., & Gaye, A. T. (2018). A model perspective on the dynamics of the shadow zone of the eastern tropical North Atlantic—Part 1: The poleward slope currents along West Africa. *Ocean Science*, 14(5), 971–997. <https://doi.org/10.5194/os-14-971-2018>
- Lathuilière, C., Echevin, V., & Lévy, M. (2008). Seasonal and intraseasonal surface chlorophyll-a variability along the northwest African coast. *Journal of Geophysical Research*, 113(C5). <https://doi.org/10.1029/2007JC004433>
- Lellouche, J.-M., Le Galloudec, O., Drévillon, M., Régnier, C., Greiner, E., Garric, G., et al. (2013). Evaluation of global monitoring and forecasting systems at Mercator Océan. *Ocean Science*, 9(1), 57–81. <https://doi.org/10.5194/os-9-57-2013>
- Lentz, S. J., & Chapman, D. C. (2004). The importance of nonlinear cross-shelf momentum flux during wind-driven coastal upwelling. *Journal of Physical Oceanography*, 34(11), 2444–2457. <https://doi.org/10.1175/JPO2644.1>
- Levin, L. A., & Breitburg, D. L. (2015). Linking coasts and seas to address ocean deoxygenation. *Nature Climate Change*, 5(5), 401–403. <https://doi.org/10.1038/nclimate2595>
- Lloyd, I. J. (1971). Primary production off the coast of North-West Africa. *ICES Journal of Marine Science*, 33(3), 312–323. <https://doi.org/10.1093/icesjms/33.3.312>
- Machu, E., Capet, X., Estrade, P. A., Ndoye, S., Brajard, J., Baurand, F., et al. (2019). First evidence of anoxia and nitrogen loss in the southern canary upwelling system. *Geophysical Research Letters*, 46(5), 2619–2627. <https://doi.org/10.1029/2018GL079622>
- Mantyla, A. W., Venrick, E. L., & Hayward, T. L. (1995). *Primary production and chlorophyll relationships, derived from ten years of CalCOFI measurements* (California Cooperative Oceanic Fisheries Investigations Reports, pp. 159–166).
- Marchesiello, P., & Estrade, P. (2010). Upwelling limitation by onshore geostrophic flow. *Journal of Marine Research*, 68, 37–62. <https://doi.org/10.1357/002224010793079004>
- Mbaye, B. C., Brochier, T., Echevin, V., Lazar, A., Lévy, M., Mason, E., et al. (2015). Do *Sardinella aurita* spawning seasons match local retention patterns in the Senegalese-Mauritanian upwelling region? *Fisheries Oceanography*, 24(1), 69–89. <https://doi.org/10.1111/fog.12094>
- Mitchell-Innes, B. A., & Walker, D. R. (1991). Short-term variability during an anchor station study in the southern Benguela upwelling system: Phytoplankton production and biomass in relation to species changes. *Progress in Oceanography*, 28(1), 65–89. [https://doi.org/10.1016/0079-6611\(91\)90021-D](https://doi.org/10.1016/0079-6611(91)90021-D)
- Montégut, C., de B., Madec, G., Fischer, A. S., Lazar, A., & Iudicone, D. (2004). Mixed layer depth over the global ocean: An examination of profile data and a profile-based climatology. *Journal of Geophysical Research*, 109(C12). <https://doi.org/10.1029/2004JC002378>
- Monteiro, P. M. S., Dewitte, B., Scranton, M. I., Paulmier, A., & van der Plas, A. K. (2011). The role of open ocean boundary forcing on seasonal to decadal-scale variability and long-term change of natural shelf hypoxia. *Environmental Research Letters*, 6(2), 025002. <https://doi.org/10.1088/1748-9326/6/2/025002>
- Monteiro, P. M. S., van der Plas, A. K., Mélice, J.-L., & Florenchie, P. (2008). Interannual hypoxia variability in a coastal upwelling system: Ocean-shelf exchange, climate and ecosystem-state implications. *Deep-Sea Research Part I: Oceanographic Research Papers*, 55(4), 435–450. <https://doi.org/10.1016/j.dsr.2007.12.010>
- Moum, J. N., Farmer, D. M., Smyth, W. D., Armi, L., & Vagle, S. (2003). Structure and generation of turbulence at interfaces strained by internal solitary waves propagating shoreward over the continental shelf. *Journal of Physical Oceanography*, 33(10), 2093–2112. [https://doi.org/10.1175/1520-0485\(2003\)033<2093:SAGOTA>2.0.CO;2](https://doi.org/10.1175/1520-0485(2003)033<2093:SAGOTA>2.0.CO;2)
- Nam, S., & Send, U. (2011). Direct evidence of deep water intrusions onto the continental shelf via surging internal tides. *Journal of Geophysical Research*, 116(C5). <https://doi.org/10.1029/2010JC006692>
- Naqvi, S. W. A., Naik, H., Jayakumar, D. A., Shailaja, M. S., & Narvekar, P. V. (2006). Seasonal oxygen deficiency over the western continental shelf of India. In L. N. Neretin (Ed.), *Past and present water column anoxia* (pp. 195–224). Springer Netherlands. https://doi.org/10.1007/1-4020-4297-3_08
- Ndoye, S. (2016). *Fonctionnement dynamique du centre d'upwelling sud-sénégalais: Approche par la modélisation réaliste et l'analyse d'observations satellite de température de surface de la mer* (PhD Thesis). Retrieved from <https://tel.archives-ouvertes.fr/tel-01481384/>
- Ndoye, S., Capet, X., Estrade, P., Sow, B., Dagorne, D., Lazar, A., et al. (2014). SST patterns and dynamics of the southern Senegal-Gambia upwelling center. *Journal of Geophysical Research: Oceans*, 119(12), 8315–8335. <https://doi.org/10.1002/2014JC010242>
- Ndoye, S., Capet, X., Estrade, P., Sow, B., Machu, E., Brochier, T., et al. (2017). Dynamics of a “low-enrichment high-retention” upwelling center over the southern Senegal shelf. *Geophysical Research Letters*, 44(10), 5034–5043. <https://doi.org/10.1002/2017GL072789>
- Peña-Izquierdo, J., van Sebille, E., Pelegrí, J. L., Sprintall, J., Mason, E., Llanillo, P. J., & Machín, F. (2015). Water mass pathways to the North Atlantic oxygen minimum zone. *Journal of Geophysical Research: Oceans*, 120(5), 3350–3372. <https://doi.org/10.1002/2014JC010557>
- Pietri, A., Testor, P., Echevin, V., Chaigneau, A., Mortier, L., Eldin, G., & Grados, C. (2013). Finescale vertical structure of the upwelling system off southern Peru as observed from glider data. *Journal of Physical Oceanography*, 43(3), 631–646. <https://doi.org/10.1175/JPO-D-12-035.1>
- Pitcher, G. C., & Probyn, T. A. (2010). *Red tides and anoxia: An example from the southern Benguela current system*. <https://doi.org/10.13140/2.1.3086.1766>

- Pitcher, G. C., & Probyn, T. A. (2011). Anoxia in southern Benguela during the autumn of 2009 and its linkage to a bloom of the dinoflagellate *Ceratium balechii*. *Harmful Algae*, 11, 23–32. <https://doi.org/10.1016/j.hal.2011.07.001>
- Pollard, R., & Read, J. (1989). A method for calibrating shipmounted acoustic Doppler profilers and the limitations of gyro compasses. *Journal of Atmospheric and Oceanic Technology*, 6(6), 859–865. [https://doi.org/10.1175/1520-0426\(1989\)006<0859:AMFCSA>2.0.CO;2](https://doi.org/10.1175/1520-0426(1989)006<0859:AMFCSA>2.0.CO;2)
- Polo, I., Lazar, A., Rodriguez-Fonseca, B., & Arnault, S. (2008). Oceanic Kelvin waves and tropical Atlantic intraseasonal variability: 1. Kelvin wave characterization. *Journal of Geophysical Research*, 113(C7). <https://doi.org/10.1029/2007JC004495>
- Rebert, J.-P. (1982). *Hydrologie et dynamique des eaux du plateau continental sénégalais (Document Scientifique—CRODT)* (p. 99). CRODT. Retrieved from <http://www.documentation.ird.fr/hor/fdi:17490>
- Risien, C. M., & Chelton, D. B. (2008). A global climatology of surface wind and wind stress fields from eight years of QuikSCAT scatterometer data. *Journal of Physical Oceanography*, 38(11), 2379–2413. <https://doi.org/10.1175/2008JPO3881.1>
- Robinson, C., Serret, P., Tilstone, G., Teira, E., Zubkov, M. V., Rees, A. P., & Woodward, E. M. S. (2002). Plankton respiration in the Eastern Atlantic Ocean. *Deep-Sea Research Part I: Oceanographic Research Papers*, 49(5), 787–813. [https://doi.org/10.1016/S0967-0637\(01\)00083-8](https://doi.org/10.1016/S0967-0637(01)00083-8)
- Rossignol, M. (1973). *Contribution à l'étude du complexe guinéen*.
- Roy, C., Cury, P., Fontana, A., & Belvèze, H. (1989). Stratégies spatio-temporelles de la reproduction des clupéidés des zones d'upwelling d'Afrique de l'Ouest. *Aquatic Living Resources*, 2, 21–29. <https://doi.org/10.1051/alr:1989003>
- Sarmiento, J. L., & Gruber, N. (2006). *Ocean biogeochemical dynamics*. Princeton University Press. <https://doi.org/10.1515/9781400849079>
- Schütte, F., Karstensen, J., Krahnmann, G., Hauss, H., Fiedler, B., Brandt, P., et al. (2016). Characterization of “dead-zone” eddies in the eastern tropical North Atlantic. *Biogeosciences*, 13(20), 5865–5881. <https://doi.org/10.5194/bg-13-5865-2016>
- Soares, P. M. M., Lima, D. C. A., Semedo, A., Cardoso, R. M., Cabos, W., & Sein, D. V. (2019). Assessing the climate change impact on the North African offshore surface wind and coastal low-level jet using coupled and uncoupled regional climate simulations. *Climate Dynamics*, 52(11), 7111–7132. <https://doi.org/10.1007/s00382-018-4565-9>
- Sylla, A., Mignot, J., Capet, X., & Gaye, A. T. (2019). Weakening of the Senegalo-Mauritanian upwelling system under climate change. *Climate Dynamics*, 53(7), 4447–4473. <https://doi.org/10.1007/s00382-019-04797-y>
- Tengberg, A., & Hovdenes, J. (2014). *Information on long-term stability and accuracy of Aanderaa oxygen optodes; information about multi-point calibration system and sensor option overview* (Aanderaa Data Instruments AS Tech. Note, 14).
- Thomsen, S., Kanzow, T., Krahnmann, G., Greatbatch, R. J., Dengler, M., & Lavik, G. (2016). The formation of a subsurface anticyclonic eddy in the Peru-Chile Undercurrent and its impact on the near-coastal salinity, oxygen, and nutrient distributions. *Journal of Geophysical Research: Oceans*, 121(1), 476–501. <https://doi.org/10.1002/2015JC010878>
- Thomsen, S., Karstensen, J., Kiko, R., Krahnmann, G., Dengler, M., & Engel, A. (2019). Remote and local drivers of oxygen and nitrate variability in the shallow oxygen minimum zone off Mauritania in June 2014. *Biogeosciences*, 16(5), 979–998. <https://doi.org/10.5194/bg-16-979-2019>
- Torrence, C., & Compo, G. P. (1998). A practical guide to wavelet analysis. *Bulletin of the American Meteorological Society*, 79(1), 61–78. [https://doi.org/10.1175/1520-0477\(1998\)079<0061:APGTWA>2.0.co;2](https://doi.org/10.1175/1520-0477(1998)079<0061:APGTWA>2.0.co;2)
- Touré, D. (1983). *Contribution à l'étude de l'“upwelling” de la baie de Gorée (Dakar-Sénégal) et de ses conséquences sur le développement de la biomasse phytoplanctonique*. CRODT. Retrieved from <http://www.documentation.ird.fr/hor/fdi:17492>
- Vaquer-Sunyer, R., & Duarte, C. M. (2008). Thresholds of hypoxia for marine biodiversity. *Proceedings of the National Academy of Sciences of the United States of America*, 105(40), 15452–15457. <https://doi.org/10.1073/pnas.0803833105>
- Villamaña, M., Mouriño-Carballido, B., Marañón, E., Cermeño, P., Chouciño, P., da Silva, J. C. B., et al. (2017). Role of internal waves on mixing, nutrient supply and phytoplankton community structure during spring and neap tides in the upwelling ecosystem of Ria de Vigo (NW Iberian Peninsula). *Limnology & Oceanography*, 62(3), 1014–1030. <https://doi.org/10.1002/lno.10482>
- Voituriez, B., & Chuchla, R. (1978). Influence of the Southern Atlantic Central Water on the distribution of salinity and oxygen in the northeast tropical Atlantic Ocean. *Deep-Sea Research*, 25, 107–117. [https://doi.org/10.1016/s0146-6291\(21\)00009-6](https://doi.org/10.1016/s0146-6291(21)00009-6)
- Voituriez, B., & Dandonneau, Y. (1974). Relations entre la structure thermique, la production primaire et la régénération des sels nutritifs dans le dôme de Guinée. *Cah. ORSTOM Sér. Oceanography*, 12, 241–255.
- Walter, R. K., Woodson, C. B., Arthur, R. S., Fringer, O. B., & Monismith, S. G. (2012). Nearshore internal bores and turbulent mixing in southern Monterey Bay. *Journal of Geophysical Research*, 117(C7). <https://doi.org/10.1029/2012JC008115>
- Walter, R. K., Woodson, C. B., Leary, P. R., & Monismith, S. G. (2014). Connecting wind-driven upwelling and offshore stratification to nearshore internal bores and oxygen variability. *Journal of Geophysical Research: Oceans*, 119(6), 3517–3534. <https://doi.org/10.1002/2014JC009998>
- Wong, S. H. C., Santoro, A. E., Nidzieko, N. J., Hench, J. L., & Boehm, A. B. (2012). Coupled physical, chemical, and microbiological measurements suggest a connection between internal waves and surf zone water quality in the Southern California Bight. *Continental Shelf Research*, 34, 64–78. <https://doi.org/10.1016/j.csr.2011.12.005>